Virtual White Matter: A Novel System for Cross-Dish Neural Interaction and Modulation

---

A Thesis Proposal

Submitted to

the Temple University Graduate Board

In Partial Fulfillment of the Requirements for the Degree

DOCTOR OF PHILOSOPHY

By Mehdi Khantan

31st of March 2025

Examining Committee Members:

Dr. Iyad Obeid, Advisor, Dept. of Electrical and Computer Engineering, Temple University

Dr. Joseph Picone, Dept. of Electrical and Computer Engineering, Temple University

Dr. Andrew Spence, Dept. of Bioengineering, Temple University

Dr. Mijail Demian Serruya, Raphael Center for Neurorestoration, Vickie & Jack Farber Institute for Neuroscience, Thomas Jefferson University

Dr. Alessandro Napoli, Raphael Center for Neurorestoration, Vickie & Jack Farber Institute for Neuroscience, Thomas Jefferson University

Abstract

Biological Neural Networks (BNNs) are characterized by complex interregional connectivity, allowing for seamless communication between different brain regions. In vitro models traditionally consist of single-dish neural cultures that cannot recapitulate the dynamics of interregional interactions. Herein, we introduce Virtual White Matter (VWM), a novel platform enabling real-time functional digital connectivity between neural cultures in separate multi-electrode array (MEA) dishes. By detecting action potentials in one dish and providing precisely timed electrical stimulation to another, VWM recreates inter-regional neural communication.

VWM represents a significant advancement in in vitro modeling by enabling controlled interactions between heterogeneous neural cultures, such as different brain regions or cell types. The platform enables the investigation of dynamic network behaviors and integration with biological and artificial neural systems. These advances will push forward biocomputing, wetware computing, and organic intelligence. Furthermore, VWM has the potential to be applied in fields like therapeutic interventions that use directed neural plasticity to promote brain injury or disease responses.

The study introduces the conceptual framework, technical implementation, and proof-of-concept validation of the VWM system. VWM enables complex in vitro models to be built with the same neural connectivity as in the human brain. VWM is versatile, placing it at the core of a transformational tool for experimental neuroscience, biocomputing, and translational research to bridge biological and digital systems.

Research Aims:

Aim 1: Develop a robust VWM platform for real-time cross-dish neural communication

Implement a proof-of-concept VWM system by establishing precise spike detection and stimulation protocols. In this setup, neural action potentials detected in the "source" dish trigger time-sensitive stimulations in the "target" dish with a fixed delay of 200 ms, creating a unidirectional connection. In a bidirectional configuration, action potentials from the target dish also stimulate the source dish, thereby mimicking interregional brain communication and laying the groundwork for more advanced neural interaction models.

Aim 2: Communicating messages between the BNNs through VWM

Aim 2 focuses on transmitting digitally coded messages between biological neuronal networks (BNNs). In this setup, a 3-bit coded message is first delivered through electrical stimulation to the first MEA, and the resulting neural activity—captured via detected spikes—is fed into a machine learning system to decode the original message. This decoded message is then used to stimulate the second MEA, whose post-stimulus spiking data is processed by another machine learning model. Finally, in a subsequent round, the message is transmitted back from the second MEA to the first, allowing comparison of the recovered code with the original to assess communication accuracy. An additional, final step will bypass the machine learning stage between the two MEAs. Instead of using a computer-based model, the timings of binned spike patterns captured from the first MEA will be passed directly as stimulation input to the second MEA. This approach effectively substitutes one BNN for the machine learning layer, enabling evaluation of how communication accuracy changes when removing computer-based decoding from the loop.

Table of Content

List of Figures

1 Introduction

1.1 Background and Motivation:

Neural tissue cultures grown in multi-electrode array (MEA) dishes are widely used to study neural network development [1], learning [2], population self-organization [3], and responses to external stimuli [4]. MEAs are a flexible and powerful tool for studying neural behavior because they can be used with different types of cells (e.g., with respect to species, genetic mutation, and brain region), different culture types (e.g., brain slices, dissociated cell cultures, organoids), and different morphologies (e.g., 2D, 3D). MEA cultures are an excellent platform for studying neural population function because they are simpler to interact with than in-vivo whole brains but also more biologically realistic than in silico simulations.

Closed-loop MEA systems [5] modify the open-loop MEA paradigm by enabling focal electrode stimulation in one region of the dish in response to detected activity in other regions. Such systems are emerging as prototypes of biocomputing, in which neural populations can be taught to respond differentially to different stimuli. These are effectively pattern recognition systems that use biological tissue instead of silicon-based computing. In the last three decades, there have been extensive efforts to leverage the processing capabilities of Biological Neural Networks (BNNs), including learning, adaptation, and information processing [6–12]. These capabilities have been used in performing specific tasks such as controlling robots [13–15], flight control [16], and playing video games [4].

Recent examples of closed-loop MEA systems include the *Dishbrain* system (Cortical Labs, Melbourne, Australia), in which both human and rodent in vitro neural networks exhibited learning behavior and goal-oriented activity when embodied in a simulated game world such as "Pong" [4]. Another example is *Brainoware* (Indiana University Bloomington), which is a live brain organoid

capable of learning and pattern detection in a 3D BNN [17]. *Brainoware* has successfully predicted a Hénon map, a fundamental non-linear dynamic system characterized by chaotic dynamics. Furthermore, Sumi et al. have used BNNs as generalization filters in reservoir computing [18], a technique that enhances the performance of tasks like speech classification and pattern recognition. Neural preparations have demonstrated potential as processing units for information, paving the way for more complex configurations of BNNs. Creating advanced forms of BNNs requires establishing connectivity between different regions or types of networks. However, the mechanisms and implications of such connectivity have not been extensively studied. The subject of this proposal, the Virtual White Matter (VWM) system, represents a pioneering effort to investigate and simulate artificial connectivity between BNNs, providing a foundation for exploring their coordinated functionality and interactions.

The VWM system extends closed-loop MEA capabilities by enabling interaction between neurons across multiple MEA dishes. As depicted in Figure 1, the VWM system electrically stimulates electrodes in a target MEA dish in response to detected action potentials in a source MEA dish. Precision timing ensures that time- and rate-based information is preserved between the dishes. The VWM paradigm allows interaction between heterogeneous cell cultures (e.g., a dish with a hippocampal rat slice can bidirectionally communicate with a dissociated knockout mouse

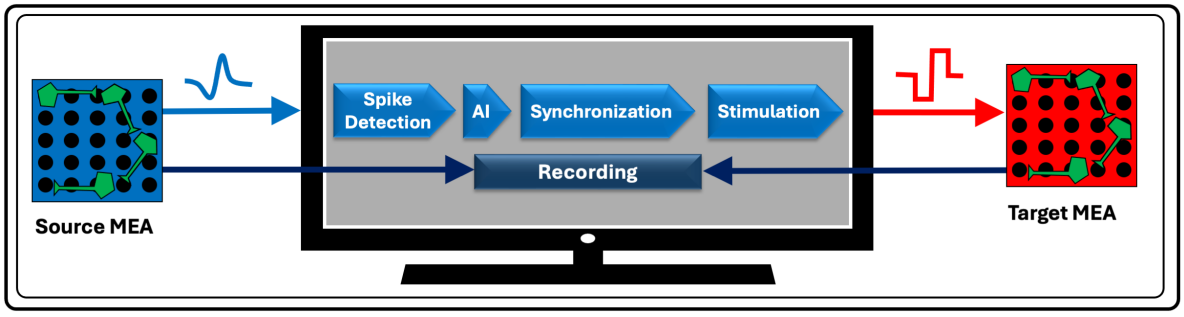

Figure 1: Schematic representation of the Virtual White Matter system.

culture). The VWM platform can also be amended to manipulate information flow between dishes as a means of probing neural coding. For example, a target dish may only be stimulated if a certain multi-electrode pattern of activity is detected in the source. The information manipulation stage could be as simple as a pass-through follower or as sophisticated as a block of artificial intelligence, allowing for a wide range of biological computing configurations.

VWM's fundamental concept is to create a functional connection between two or more neural cultures on distinct MEA dishes in the digital world. More precisely, using VWM, one could modulate the activity of an active target neural setup in real time by providing stimulation that is contingent upon the neural activity of the source neural setup. This real-time interaction mimics the way different regions of the brain communicate with each other, allowing for the study of how changes in one region can influence another. Early closed-loop systems provided the foundation for this approach by demonstrating that recorded neural activity from one region could dynamically trigger stimulation in another, effectively providing an auxiliary interregional brain communication [19]. Building on these principles, VWM not only replicates such interactions but also offers a platform for precisely controlling and manipulating the timing and pattern of information flow, enabling deeper investigations into neural coding and plasticity.

This platform has the potential to enable user-modulated communication between multiple heterogeneous cultures, which vastly expands the complexity of neural modeling. To date, most research on BNNs has focused on single neural preparations, and little effort has been made to interconnect multiple BNNs to process information through a hybrid interconnection of the biological and digital systems. The VWM addresses this gap by enabling interconnections that could bridge multiple BNNs and ANNs, a prerequisite for biocomputing, wetware computing, and organic intelligence [17,18,20–25]. Furthermore, the utilization of closed-loop stimulation

systems in therapeutic environments has been investigated, with the potential to provide interventions for neurological disorders. Such applications can aid in recovery from injury or disease by directing the plasticity of the nervous system through real-time neural circuit modulation. VWM has the potential to study and replicate phenomena such as "virtual strokes," "white matter disconnection" [26,27], or “brain rewiring” [28] by selectively modulating or disrupting communication between neural populations.

Furthermore, VWM can serve as a foundational building block for implantable brain-computer interfaces (BCI), enabling reciprocal linking between spatially distant recording and stimulation elements [29]. It also offers the potential to reconstruct entire mammalian brain models by interconnecting separate sections of their brain in vivo. This will enable the creation of more elaborate multi-specimen transfer functions or biological transformers, surpassing the capabilities of single isolated specimens. Ultimately, VWM can be a fundamental building block for virtual embodiment, in which several linked specimens could be collectively embodied in a virtual environment or in a robotic body.

This study consists of two phases. In the first phase, a proof-of-concept version of the Virtual White Matter (VWM) system has been implemented. Initially, spontaneous neural action potentials (spikes) detected in the "source" dish were used to trigger stimulations in a "target" dish with a fixed delay of 200 ms. Subsequently, machine learning techniques classified the source of stimulation based on post-stimulus spike patterns in the "target" dish. This phase was further expanded to include bidirectional communication between the two dishes by relaying post-stimulus spikes induced in the "target" dish back to the "source" dish. The continuous feedback loop established in this manner functions autonomously, emulating interregional brain

communication and providing a foundation for exploring more complex neural interactions in future research.

In the second phase, the study transitions from spontaneous neural activity to a coded message introduced into the system and subsequently identified. The message is first encoded on the first MEA and recognized via a machine learning algorithm that processes spike patterns detected in that same MEA. These spike-derived codes are then transmitted to the second MEA as stimulation signals, where they are similarly decoded by analyzing post-stimulus evoked spike patterns. This unidirectional communication setup provides a baseline for comparative analysis of encoding-decoding accuracy.

Subsequently, to evaluate bidirectional communication, the decoded message on the second MEA is re-encoded and sent back to the first MEA. Demonstrating successful decoding of this return pathway confirms the ability of the VWM system to support robust two-way communication. Finally, in a bypass step, the computer-based decoding between the two MEAs is omitted: rather than employing machine learning, the binned spike outputs from the first MEA are sent directly as stimulation signals to the second MEA, effectively using the second BNN itself as the "decoder." This final test reveals how communication accuracy changes when the machine learning pipeline is removed, further underscoring the potential of the VWM approach for interconnecting established BNNs and facilitating integrated neural network architectures.

1.2 Biology of Neurons

1.2.1 Structure of Neurons

Neurons, the fundamental units of the nervous system, communicate through electrical and chemical signals. Each neuron consists of three main structures: the cell body (soma), dendrites, and the axon as shown in Figure 2a. The soma houses the nucleus, which contains the genetic material essential for neuronal function and survival. Dendrites serve as the input zone, receiving

signals from other neurons, while the axon transmits these signals to target cells. Axons vary in length, ranging from a few millimeters in the brain to several feet in the spinal cord. They may branch extensively (from 10 to 250,000 branches) to reach multiple target cells. The ends of these branches form axon terminals, where neurotransmitters are released to propagate the signal.

1.2.2 Neuronal Communication

The electrical properties of neurons arise from the distribution and movement of ions across the cell membrane. Key ions involved in this process include negatively charged proteins (large anions) and chloride ions (Cl^-), as well as positively charged sodium (Na^+) and potassium (K^+) ions. These ions create an electrochemical environment that determines the neuron's ability to generate and transmit signals.

Neuronal membranes contain specialized channels that regulate the ion movement. Two key types are leaky channels, which allow continuous ion flow, and voltage-gated channels, which open and close in response to voltage changes through the cell membrane. Potassium (K^+) is more concentrated inside the neuron, while sodium (Na^+) is more concentrated outside. Due to the concentration gradient, potassium tends to leave the cell, but the electrical gradient pulls it back in, maintaining equilibrium. Similarly, sodium follows its own electrochemical gradient.

Neuronal communication occurs through neurotransmitters, which are chemical messengers released from the presynaptic neuron. Examples include:

- Dopamine is involved in various functions, including motor control, motivation, and reward processing.
- Acetylcholine (Ach) is commonly used by motor control neurons to communicate with muscles, facilitating movement.

- Endorphins, a class of neurotransmitters, play a role in pain relief, stress reduction, and the regulation of mood and immune response.

These neurotransmitters bind to ligand-gated receptors on the dendrites of the postsynaptic neuron, triggering an excitatory postsynaptic potential (EPSP) or an inhibitory postsynaptic potential (IPSP) depending on the type of receptor and ion channels involved. These neurotransmitters are only released into the synaptic cleft upon the arrival of an action potential. EPSPs make the neuron

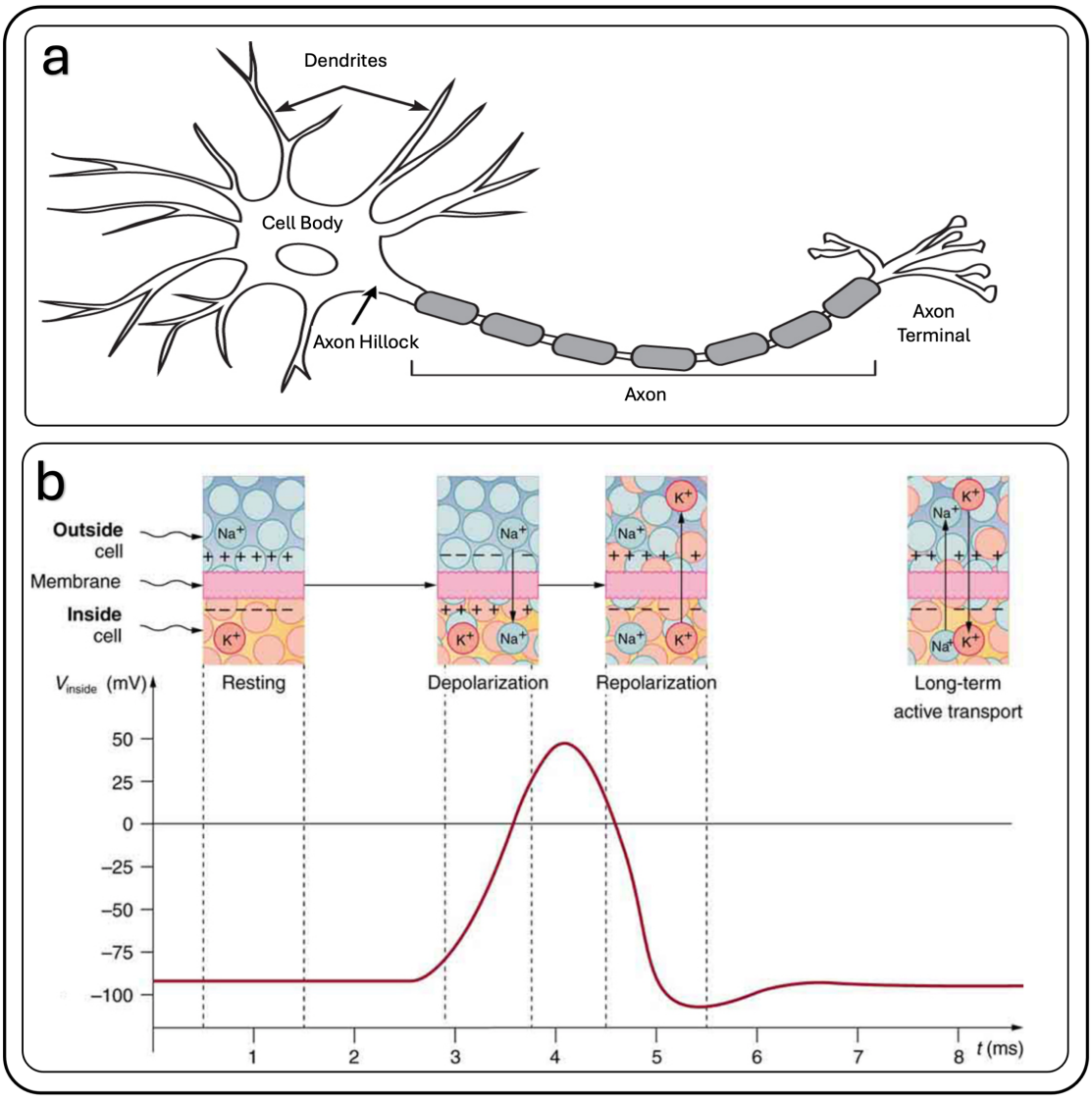

Figure 2: Neuronal Architecture and action potential stages a) Different parts of a neuron. b) Neuron membrane voltage during an action potential and the activation of different ion channels.

more likely to fire, while IPSPs inhibit it. The axon hillock, a specialized region connecting the soma to the axon, functions as a decision-making center. If the sum of incoming EPSPs surpasses IPSPs and reaches the threshold of approximately -55 mV, an action potential is initiated. This all-or-nothing response ensures the uniform propagation of the signal. When a neuron fires, that is essentially a spatial and temporal integration of information from upstream neurons.

An action potential propagates along the axon, and when it reaches the axon terminals, neurotransmitters are released into the synaptic cleft, continuing the cycle of neuronal communication.

The stages of membrane potential changes during an action potential are shown in Figure 2b:

- Resting Potential (about -70 mV): The neuron is at rest. The membrane voltage is maintained by sodium-potassium pumps, which exchange three Na^+ ions out of the cell for two K^+ ions into the cell (producing a net negative voltage), and by leaky channels that allow passive ion movement.
- Depolarization (+30 mV): When the membrane potential reaches the threshold (~ -55 mV), voltage-gated Na^+ channels rapidly open within less than 1 millisecond, allowing Na^+ to rush into the cell. These channels have a fast activation gate that responds almost instantly to voltage changes, leading to a rapid rise in membrane voltage.
- Repolarization: At peak depolarization (+30 mV), voltage-gated Na^+ channels inactivate via a built-in inactivation gate, which blocks further Na^+ influx. At the same time, voltage-gated K^+ channels begin to open, but at a slower rate (~2-5 ms delay) compared to Na^+ channels. This delayed opening allows K^+ to exit the cell, restoring a negative membrane potential.

- Hyperpolarization (< -70 mV): Because K^+ channels close more slowly than Na^+ channels, delayed rectifier K^+ channels remain open for a short period after repolarization, causing the membrane potential to temporarily become more negative than resting levels.
- Restoration: Once K^+ channels finally close, the sodium-potassium pump actively restores ion balance by pumping Na^+ out and K^+ back into the cell, bringing the membrane potential back to its resting state.

These molecular mechanisms highlight how the specific biophysics of membrane proteins shape neuronal electrical activity and how even minor alterations, such as genetic affecting ion channel functions, can lead to profound physiological consequences. These include epilepsy, certain migraines, and long QT syndrome as well as neuromuscular disorders, chronic pain conditions, neurodevelopmental diseases, and neurodegenerative disorders [30–32].

1.3 Microelectrode Arrays

1.3.1 How Microelectrode Arrays Work

Microelectrode arrays (MEAs) integrate electrodes into in vitro neural cell cultures to detect their extracellular electrical signals and to deliver targeted electrical stimulation. The functionality of MEAs is based on the electrophysiological properties of excitable neurons. Neurons generate ionic currents across their membranes, leading to extracellular voltage fluctuations that MEAs can detect. During recording, these electrodes sense voltage changes in the extracellular medium and convert them into electronic signals. During stimulation, they deliver electrical pulses, which generate ionic currents in the surrounding medium that modulate neural activity. The quality of recordings depends on multiple factors, including electrode geometry, impedance, and the quality of cell-electrode coupling.

When an electrode is placed in an ionic solution (such as a neural culture medium or cerebrospinal fluid), an electrical double layer forms at the interface due to charge redistribution. This interface

behaves as a capacitor but also exhibits resistive properties, which influence signal quality and impedance. The first layer, which is the electrode surface, carries free-moving electrons, as it is a metal. The second layer is the electrolyte side, in which ions in the surrounding solution rearrange in response to the electrode's charge. These two layers of opposite charges act just like the two plates of a capacitor — one plate being the electrode's surface and the other being the charged ions in solution [33].

MEA recordings capture either action potentials representing activity from a single neuron or local field potentials (LFPs), which are low frequency fluctuations representing activity from multiple neurons. While all extracellularly recorded action potentials share a similar shape (a negative version of the neuron's membrane voltage that was shown on Figure 2b) their amplitude varies based on neuron size, axon properties, ion channel composition, media conductivity, and the distance between the neuron and the electrode. Larger neurons with thicker axons generate higher voltage in vicinity of their membrane, and this voltage attenuates approximately with the inverse of distance from the membrane of the cell [34].

Depending on electrode size and neuronal density, a single electrode can record signals from multiple nearby neurons, resulting in overlapping extracellular voltages. Researchers use mathematical techniques such as spike sorting to separate these signals, though this process can be computationally demanding [35,36]. To ease the signal isolation process, high-density MEAs with smaller and less electrode pitch (center-to-center distance between the conductive areas of two electrodes) have been developed, positioning each electrode closer to individual neurons and covering all essential neuronal space. These designs enhance spatial resolution by reducing the number of neurons contributing to each electrode's signal. However, decreasing the size of the electrodes increases their impedance which in turn makes the captured signal weaker and more

susceptible to noise. Addressing these challenges requires amplifiers with higher input impedance (on the order of hundreds of megaohms) and the adding some software techniques for signal processing to remove the unwanted noise. A new method for spike detection has been devised and is discussed in detail in Section 2.4 Realtime Spike Detection.

1.3.2 Materials and Fabrication:

Microelectrode arrays are built from biocompatible conductive materials and insulating substrates that together determine their performance and longevity. Noble metals like platinum (Pt) and gold (Au) are commonly used because they resist corrosion and are biologically inert [37]. Platinum-iridium alloys (Pt-Ir) and iridium (often as iridium oxide, IrO_2) are also widely used for their high strength and high charge-injection capacity [38]. In contrast, materials like copper or silver are avoided despite excellent conductivity, since they corrode or leach toxins in tissue [37]. To improve signal quality, electrode surfaces are often coated to lower impedance: for example, depositing platinum black, iridium oxide, or titanium nitride (TiN) can reduce a 50 μm electrode's impedance to ~10–20 kΩ at 1 kHz

1.3.3 In-Vitro Microelectrode Arrays

Planar MEAs used for in vitro research are typically transparent MEAs with a grid of microelectrodes embedded in a dish or slide, allowing neurons or cardiac cells to grow over the electrodes. A common configuration is a roughly 6×10 or 8×8 electrode grid (60–64 electrodes total) covering a few square millimeters. For example, the MED64 (Alpha MED Scientific, Osaka, Japan) probe (Figure *3*a) has 64 electrodes with electrode sizes of 20 μm or 50 μm and arranged with center-to-center spacings of 100–450 μm. These electrodes are typically flat pads made of noble metal or conductive ceramic. Indium tin oxide (ITO) film is often used for the underlying tracks due to its transparency, and the electrode sites are coated with a low-impedance material

like platinum black or TiN. TiN-coated electrodes 30 μm in diameter have impedance on the order of 100 kΩ at 1 kHz, while 50 μm Pt-black electrodes can be 20 kΩ, yielding an excellent signal-to-noise ratio for extracellular spikes. Planar MEAs often include large reference electrodes (typically in the 4 corners of the array) and can support stimulation on any site. These dish-based MEAs allow long-term recordings from cultured networks or acute brain slices and can be reused a handful of times with proper care [39]. More recently, high-density CMOS MEAs have greatly expanded in vitro capabilities. In these devices, each electrode is integrated with on-chip amplifiers and multiplexers, enabling thousands of electrodes to be recorded simultaneously. A prime example is 3Brain's (Pfäffikon SZ, Switzerland) high-density MEA: a 4096-electrode array on a 2.7×2.7 mm silicon chip, arranged as a 64×64 grid. Each electrode on this CMOS-MEA is only 21 μm square with a 42–60 μm pitch, and all 4096 channels can be read at 1 kHz [40]. This technology achieves sub-cellular resolution, essentially "imaging" electrical activity without a microscope. The BioCAM DupleX system [41] records from 4096 electrodes in parallel, capturing both single-neuron spikes and local field potentials propagation across brain slices. Materials for CMOS MEAs must be fully integrated – 3Brain uses platinum-coated electrodes on CMOS to ensure biocompatibility and low noise.

1.3.4 In Vivo Microelectrode Arrays

In vivo MEAs are specially designed for implantation, either sitting on the surface of neural tissue or penetrating it to record extracellular activity. They are generally categorized by form-factor: microwire arrays, silicon microfabricated arrays (e.g. Michigan and Utah probes), and flexible polymer arrays. These devices differ in electrode density, geometry, and tissue response.

Microwire MEAs consist of fine wires (typically 30–50 μm diameter) inserted into the brain, often bundled in arrays of 4 to 64 or more. The wires are insulated (with polyimide, parylene, glass, or

Teflon) except at the tip, which serves as the recording site [37]. Common materials are tungsten, stainless steel, or Pt/Ir wires, chosen for stiffness to penetrate brain tissue yet resilience against bending. Each wire records spiking activity from neurons in a small 50–100 µm

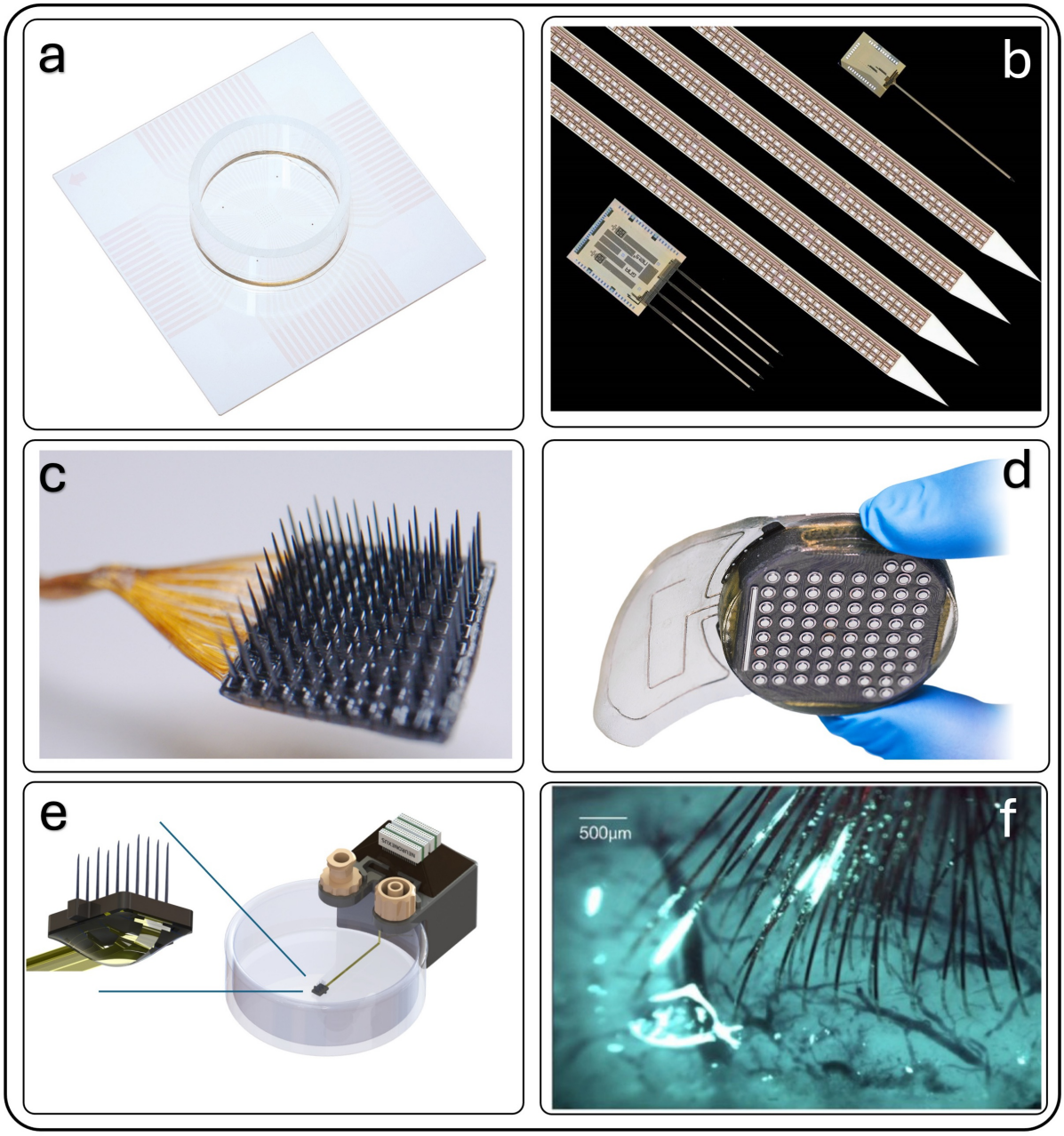

Figure 3*: Different forms of Micro Electrode Arrays (MEAs).a: MED-64 plainer MEA for in-vitro and in-vivo applications. b: Neuronexus Michigan Arrays in-vivo animal studies. c: Blackrock Neurotech Utah array for human studies. d: WIMAGINE ECoG Array for human studies e: Proposed MEA system for ex-vivo studies. f: Neuralink flexible electrodes implanted in a rat.*

radius volume around its tip. Variants like tetrodes (four twisted microwires) improve single-unit isolation by recording each neuron on multiple closely spaced tips.

Silicon-based MEAs are fabricated by MEMS processes, yielding more complex geometries and higher site counts on rigid shanks. There are two classic designs, named for the universities where they were developed. Michigan Arrays are planar polysilicon or silicon probes with multiple recording sites distributed along the length of a thin shank. Each Michigan probe is typically 15 μm thick and 50 μm wide, with a sharp tip, and several electrode contacts (pads of 10–20 μm) arranged in different forms from tip to base as shown in Figure *3*b. Probes can also have multiple shanks: e.g. a 4-shank device with eight electrodes per shank yields 32 channels in one implant [37]. The rigid silicon substrate minimizes bending during insertion, giving precise electrode placement. Their advantage is the ability to capture laminar activity profiles – recording neurons at different depths (multisite vertical recordings to study cortical columnar activity, etc. However, the flat shank can cause more tissue damage and displacement than thin wire, and the high channel count can introduce crosstalk due to inter-track capacitance [37]. Modern versions include on-shank electronics: the Neuropixels (Leuven, Belgium) probe is essentially a CMOS-Michigan hybrid, with 960 recording sites on a 10 mm length shank, 70 μm wide [42]. In Neuropixels, 384 sites can be selected to record at once (out of 960), and integrated amplifiers allow this enormous scale without overwhelming noise. This represents an order-of-magnitude leap in channel count, enabling brain-wide recordings with single-cell resolution in rodents. Those being said, Michigan arrays have evolved from early 16-channel probes to state-of-the-art 1000-channel microsystems, all leveraging silicon microfabrication for precision and density.

In contrast to the thin planar Michigan style, the Utah array is a 3D bed-of-nails configuration. It consists of a grid of silicon needles (typically 100 needles in a 10×10 array over a 4 mm×4 mm

area) etched from a single silicon block. Each needle is around 80μm radius at the base and tapers to a sharpened tip (around 1μm tip radius), with single metal electrode site located at the tip. All needles are the same height (commonly 1.0 or 1.5 mm for cortex) so that the array records from approximately one cortical layer (a horizontal array of sites at uniform depth). The electrodes are connected via metallization through the base to a connector (e.g. a ceramic CerePort of BlackRock Neurotech, Utah, USA) [43]. The standard Utah array, commercialized by Blackrock Microsystems, has 96 active electrodes (4 corner needles are often inactive for mounting) and is FDA-approved for human research which is shown in Figure *3*c. Key specifications include a 400μm inter-electrode pitch, needle length options from 0.5 mm up to 1.5 mm, and tip metallization with platinum or iridium oxide. The Utah array's design enables recording from hundreds of neurons simultaneously, since each microelectrode can pick up multiple units in its vicinity and the array spans a broad surface area (e.g. 4 × 4 mm of cortex). It has been used in many brain-machine interface demonstrations; for example implanted Utah arrays in motor cortex have allowed humans to control robotic arms [44–46] or detect handwriting [47,48,48].. The array is also used in neuroscience for recording population activity and in neuro prosthetics for stimulation (each needle can deliver localized microstimulation) [49]. Utah arrays are considered the "gold standard" for multi-unit cortical recordings, with over two decades of use and over 20,000 citations in the literature [37].

In general, the Michigan and Utah arrays are regarded as state-of-the-art penetrating MEAs and represent two paradigms. The Michigan array provides precise vertical sampling with multiple electrodes per shank, whereas the Utah array maximizes horizontal coverage with a single electrode per shank and numerous shanks. The Utah arrays, which are commercialized by Blackrock Microsystems, have been approved by the FDA for human implantation and are now

used in clinical research settings. In contrast, the Michigan arrays have not been approved for human clinical use and are primarily used in animal studies [37,50].

Flexible Arrays replace rigid silicon or metal based MEAs with polymer materials (e.g. polyimide, Parylene, SU-8) that better match the brain's stiffness. The motivation is to minimize chronic tissue reaction caused by micromotion of a stiff implant against softer neural tissue. Flexible arrays can bend and move with the brain, causing less strain and inflammation over time The stiffness of the materials is being measured by Young's modulus (E) which is a property of the material that tells us how easily it can stretch and deform and is defined as the ratio of tensile stress (σ) to tensile strain (ε). Stress is the amount of force applied per unit area ($\sigma = F/A$) and strain is extension per unit length ($\varepsilon = dl/l$). Young's modulus of polyimide is around 2.5 GPa vs silicon's is around 200 GPa, which shows their difference in terms of stiffness, while the brain tissue is much softer (E = 0.4–15 kPa) [51]. The mismatch between the stiffness of the brain tissue and the implanted microelectrode can lead to low and long-term inflammation due to micromovements of the brain tissue [37,52,53].

Typical examples include thin-film polyimide probes with metal traces (often gold or platinum) with multiple electrodes on each shank similar to Michigan probes, but only 5–20 μm thick and with significantly reduced stiffness.

Another category is surface-conforming arrays, such as electrocorticography (ECoG) grids, which are made of silicone or polyimide with embedded electrodes placed on the brain surface. However, these arrays record local field potentials rather than individual spikes. ECoG is a neural recording technique that uses surface electrodes positioned directly on the cortical surface to measure electrical activity. ECoG arrays are commonly used in clinical settings for pre-surgical epilepsy mapping and have recently gained attention in research on brain-computer interfaces (BCIs) [54].

A sample of these MEAs is shown in Figure *3*d. ECoG arrays are classified as subdural electrodes, meaning they sit on the exposed brain surface without penetrating tissue. The electrode contacts are typically made of platinum-iridium (Pt-Ir) or gold (Au) and are embedded in a flexible, biocompatible polymer substrate such as silicone, polyimide, or Parylene-C.

Another notable design is Neuralink's thread-like electrodes [55]: ultra-fine polyimide filaments (around 5–6 μm width) with embedded gold traces and 32–64 recording sites along each filament as shown in Figure *3*f. The stiffness of the threads are so low that they cannot be inserted by themselves so Neuralink developed a micro-surgical robot [56] to insert them reliably into cortex. Once implanted, their flexibility virtually eliminates large micromotion forces, greatly reducing vascular damage (the robot can avoid blood vessels with micron precision) and inflammatory responses.

1.3.5 Custom Ex-Vivo Microelectrode Arrays

In addition to conventional in-vitro and in-vivo MEAs, we developed and evaluated a new generation of 3D ex-vivo MEA systems for recording and stimulating neural tissue preparations, including brain slices (see Figure *3*e). While these 3D MEAs were not used in the present study, they will be implemented in future VWM development. We acquired Neuronexus Michigan Array Shanks (Model 4x8-prox-2mm-150-400-177, Neuronexus, Ann Arbor, MI, USA) and positioned them upright to allow brain slices to be placed and gently penetrated onto the shanks. Additionally, we designed a custom dish holder with an integrated automatic media exchange system, enabling continuous media change. This setup facilitates simultaneous neural recording and stimulation while optimizing conditions for long-term activity monitoring.

2 System Setup

2.1 Cell Preparation

To conduct Aims 1 & 2, we culture dissociated neural cells in MEAs for 14 to 50 days on the MED64 electrodes. Cortical neurons were isolated from embryonic day 18 (E18) rat cortices in a protocol approved by the Institutional Animal Care and Use Committee (IACUC). The cells were plated onto MED64 P515A 8x8 Probe MEAs, which feature 50*50 μm^2 electrodes spaced 150 µm apart. Prior to cell placement, the MEAs were coated with a 20 µg/ml solution of poly-D-lysine (PDL) to enhance cell adhesion. After a 30-minute incubation, the PDL solution was removed, and the MEAs were rinsed three times with sterile water to eliminate any excess. A 2 µg/ml laminin

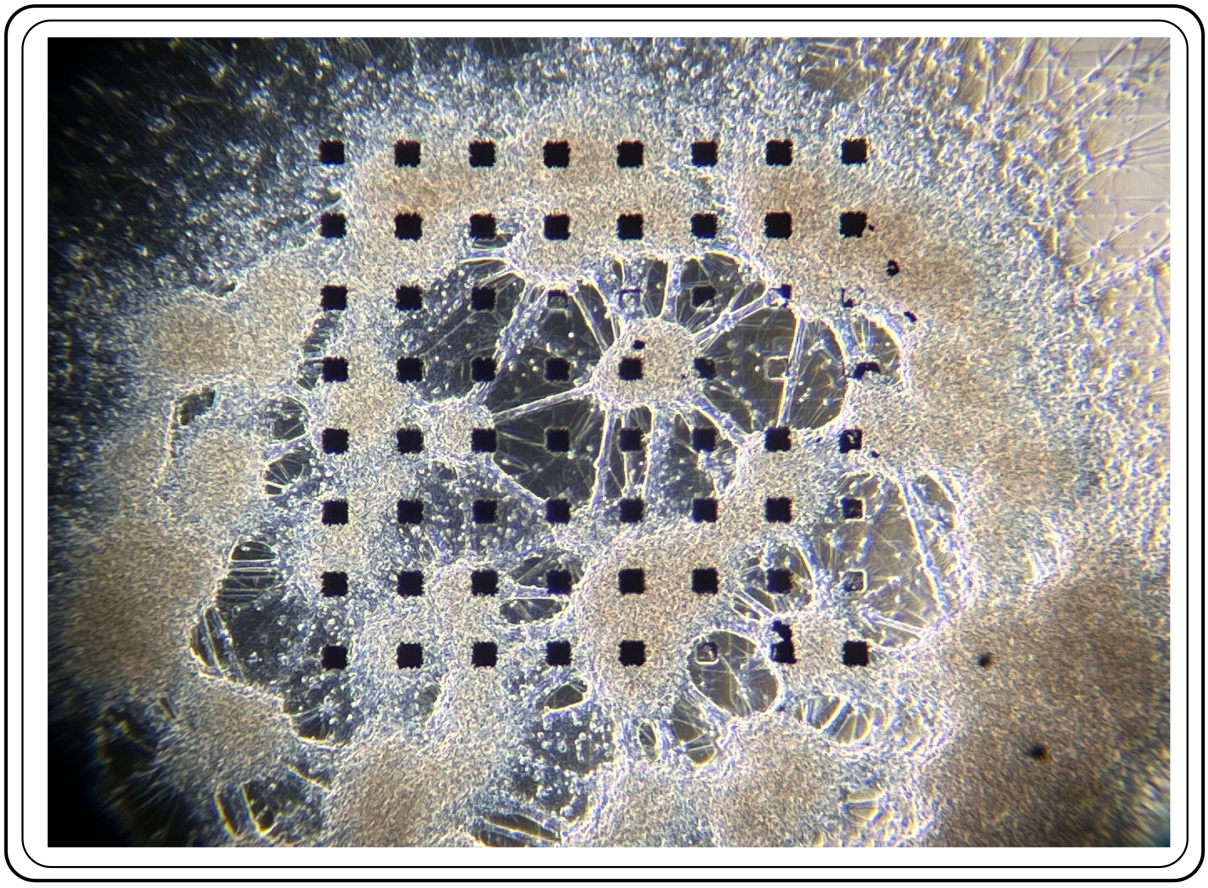

Figure 4:Microscopic image showing neural cell placement on the MEA

solution was then applied to the MEAs, incubated for 30 minutes, and subsequently removed, followed by three additional rinses with sterile water. Approximately 50,000 cortical neurons were plated onto each MEA and were maintained in an incubator at 37 ◦C with 5% CO2. The cells were maintained in Neurobasal-A medium supplemented with B-27 and GlutaMAX (referred to as NB Active 4 media). The culture medium was refreshed by replacing approximately 60% of the volume twice per week. Neural activity within the cultures typically began to manifest around day 14 post-plating and was sustained until approximately day 48. Figure 4 shows a microscopic picture of the cells on the MEA 30 days post plating.

2.2 The MEAs

For this study, dissociated neural cells from rat cortex were used. To culture, record, and stimulate these cells, the MED-64 system, a commercial 2D in vitro MEA platform, was used. The MED-64 MEA contains 64 planar microelectrodes arranged in an 8×8 grid placed on a glass plate, each with a diameter of approximately 50 µm, spaced 150 µm apart, and housed in a 10 mm-high package, enabling multi-site measurement of neuronal activity in organotypic slice cultures, dissociated cells, and tissue slices. These electrodes are fabricated from platinum for their low impedance and stability, coated with platinum black for lowering the impedance and increasing signal quality.

2.3 Data Acquisition and Electrical Stimulation System

A top-level system block diagram is shown Figure 5. Each MEA contains 64 electrodes, and the system simultaneously interfaced with two MEAs. The MEAs were placed in an MEA connector (MED-C03, Alpha MED Scientific) and connected to the recording and stimulation system via custom adapters. The PCB of the adaptors have been designed through Altium Designer software and hand soldered after printing. These custom adapters bridged the mounting hardware to the Intan headstages to create a 64-channel bidirectional link for each MEA. For each MEA, two 32-

channel Intan (Los Angeles, CA) M4032 RHS stim/record headstages were used to perform both data recording (with sampling rates of up to 30 kSamples/s) and electrode stimulation (current-controlled).

Since the system interfaced with two MEAs, a total of four 32-channel headstages were employed, fully utilizing the 128-channel capacity of the Intan system. A bidirectional link connected the headstages to a 128-channel controller unit (RHS, Intan), which in turn relayed data and control to a personal computer via USB. The acquisition computer used a conventional multithreaded architecture to run in parallel the stock Intan software I/O package (RHX) for acquisition system management and data acquisition and a custom VWM Software for real-time data processing and stimulation control (see (a)). These parallel application threads communicated via a local TCP socket. Once the VWM software detected a spike in the source dish that met certain criteria, a stimulation command was passed to an ARM microprocessor (STM32F410, STMicroelectronics, Plan-les-Ouates, Switzerland), which synchronized and buffered stimuli across channels before triggering the controller to stimulate the target MEA. An I/O expander (E6500, Intan) provided

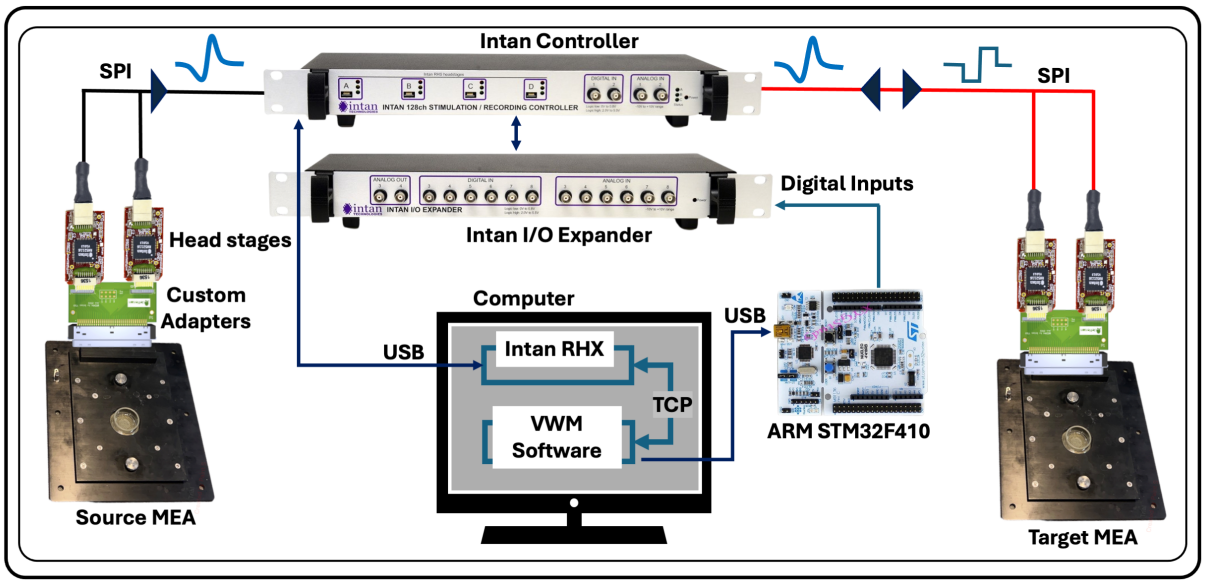

Figure 5: Block diagram of the Virtual White Matter (VWM).

supplemental digital I/Os, enabling seamless relay of stimulation commands from the microcontroller to the Intan controller.

To deliver stimulation patterns to the Intan head stages, two primary methods can be employed. The first is to send stimulation commands through the TCP Command Port. Testing revealed that the delays associated with this method due to transmission through the TCP Command Port, Intan RHX software, and the universal serial bus (USB) were inconsistent. To achieve consistent delays, a second method was developed in which stimuli were digitally triggered through the I/Os of the Intan expansion box. This method required the use of an STM32F407 microcontroller, receiving stimulation commands through USB, with an onboard circular buffer implemented to compensate for any timing inconsistencies in data recording or software-based signal processing. The circular buffer allowed asynchronous data input and synchronous output, ensuring precise timing.

Prior to stimulation, the VWM software preprograms the stimulation parameters—including pulse shape, amplitude, pulse width, number of pulses, etc.—into the Intan controller. The stimulation trigger of each target electrode is assigned to a digital input signal on the Intan expansion box. The microcontroller generates these triggering pulses based on the commands received from the VWM software via USB in real time. Each rising edge of a pulse on the expansion box's digital input activated the preprogrammed stimulation on the corresponding electrode, with the expansion box relaying the stimulation triggers to the Intan controller. This entire synchronization process occurred within the firmware of the microcontroller and the Intan system, avoiding variability associated with operating systems and ensuring consistent timing. The final stimulation commands were transmitted to the headstages via Serial Peripheral Interface (SPI) cables.

To minimize stimulation-induced artifacts and amplifier railing—which occurs when stimulation voltages exceed the system's maximum readable voltage (6.4 mV for the Intan RHS system)—

some neural recording devices offer blanking hardware features, namely the capability to completely turn off the amplifier and zero out the recording for a predefined time both pre- and post-stimulus to reduce artifacts caused by stimulation. However, this approach could potentially destabilize IIR filters due to DC-offset issues during the initiation phase following the zero-out period. Since this feature is not available in the Intan system, an alternative method was employed to address these artifacts. The Intan system was configured to temporarily reduce the amplification gain across all electrodes of the stimulated head stage during the stimulation. While a low-pass filter (with Intan's default setting at 1000 Hz) is commonly used to filter out these high-frequency

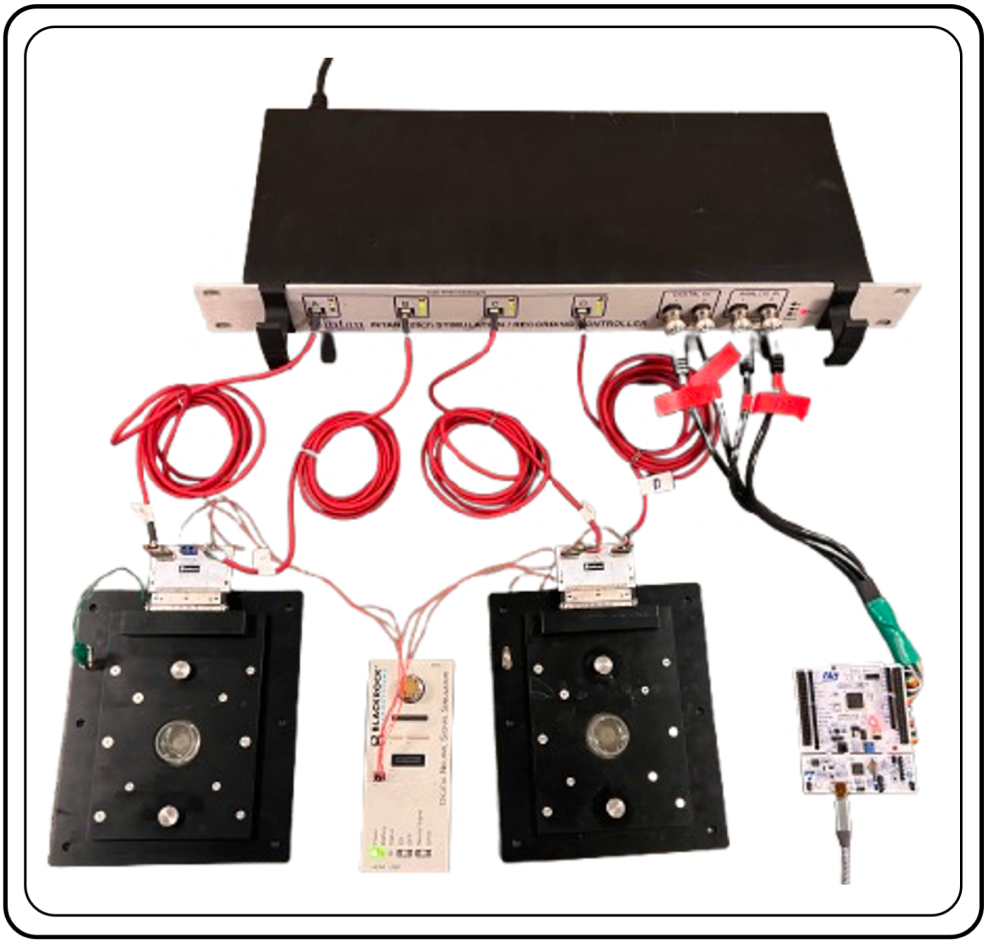

Figure 6: Experimental setup for testing signal processing and spike detection

artifacts, it proved impractical because the initiation of the filter prior to stimulation introduced start-up artifacts, especially in the presence of residual DC voltage from previous stimulations. By instead reducing the amplification during stimulation, these issues were mitigated, leading to more accurate signal detection and reduced artifact impact [57].

Before working with actual neurons on the MEA, we developed a minimal bench simulation system, as shown in Figure 6. This system utilized a Blackrock Digital Neural Signal Simulator (PN-8282, Blackrock Microsystems, LLC, Salt Lake City, UT) to generate simulated neural activity. The simulator produced a baseline of low-frequency activity along with various modes of high-frequency spikes, including phases of normal single spikes and bursts. The outputs from the Digital Neural Signal Simulator were connected to the MEA inputs, simulating neural activity within the dish. This setup allowed us to develop and refine the system efficiently, minimizing the time spent on cell culturing and experimental preparation.

2.4. VWM Software

Figure 7a shows a detailed block diagram of the custom VWM software package and its interaction with the external hardware components. The software was written in standard Python 3.0 for ease of implementation and portability between operating systems. The code is sufficiently lightweight to perform real-time signal processing on up to 4 source and 4 target channels with recording from up to 128 channels running on a Windows 11 PC equipped with a 12th Gen Intel(R) Core (TM) i9-12900K processor and 64 GB of RAM. On startup, the VWM software preconfigures the Intan RHX software to initiate data collection and prepares the Intan controller hardware to receive stimulation triggers from the microcontroller via the I/O expander. The RHX software streams raw signals from 128 channels via a local TCP socket and transfers a user-defined subset of channels to the VWM software for real-time processing while also storing all data into dedicated files for

optional offline analysis. TCP communication can, however, introduce unpredictable latencies and data packets can be received in different chunk sizes due to packet handling and operating system overhead. These latencies can degrade the communication of rate-encoded spike data between the source and target MEAs [58,59]. To mitigate these issues, the VWM software uses a circular data buffer. Namely, raw signal data is asynchronously pulled by the read thread and written into the circular buffer in variable-sized chunks as received via TCP. The signal processing thread then retrieves the data from the circular buffer in fixed chunk sizes, equivalent to 25.6 ms of data, ensuring consistent processing times and minimizing the effects of irregular delays between consecutive data chunks. The signal processing thread applies a user-defined band-pass Infinite Impulse Response (IIR) filtering (250-5000 Hz, Butterworth, 3rd order) followed by a custom spike detection module (see Section Realtime Spike Detection). Spike times were passed to the artificial intelligence (AI) module, which can be programmed to only trigger stimulations (see Section Stimulation) in the target MEA when source spikes meet certain user-defined criteria (e.g., channels 1 and 7 fire within 25 ms). For testing purposes, the AI was configured as a pass-through, meaning that every detected source spike triggered a matching stimulation in the target MEA.

2.4 Realtime Spike Detection

A real-time multi-threshold window discriminator spike detection system was customized specifically for the MEA signals observed in our dissociated neuron preparations. The algorithm continuously monitors incoming data, identifying potential spikes when a signal crosses a negative threshold (-A) and subsequently a positive threshold (+B). If the time between these crossings is less than T1 or greater than T2, the event is classified as an artifact. Otherwise, the system waits for the signal to cross the zero. If the zero-crossing time falls within the range of T3 to T4, the event is classified as a spike, and as an artifact otherwise. Furthermore, the signal must not exceed ±C within a 1-millisecond window prior to crossing -A and 2 ms after. Some examples of the spike

detections and artifact removals have been illustrated in Figure 7b and the pseudocode is on Figure 7c.

All the above-mentioned parameters, namely, spike detection thresholds and time windows, were determined by an offline meta-analysis of data previously collected from six MEA preparations of E18 rat dissociated cortical neurons. In more detail, a simple threshold (4 times the background RMS level) was used to detect events, which were in turn reduced using PCA and clustered using K-means. Clusters of spikes were differentiated from clusters of artifacts and noise and used as templates for tuning the spike sorting parameters A, B, C, T1, T2, T3, and T4. Results were consistent across all six MEAs. Threshold A and B were set, respectively to, 5.5 times and 2 times the background RMS of each channel. RMS levels for each electrode were determined over a 4-second period at the start of the experiment. Threshold C was fixed at ±70 μV, with T1, T2, T3, and T4 set to 0.2 ms, 0.6 ms, 0.25 ms, and 1 ms, respectively. These values were chosen based on the experimental setup and cell types and may vary under different conditions. It is important to note that in the target dish, the stimulus-induced responses predominantly manifested as bursting activity, which did not exhibit the typical morphology of individual spikes. Unlike conventional spikes, the shape of spikes within bursts is more variable and less defined, making them less suitable for the proposed algorithm, which performed better with distinct individual spikes. To address this, both the proposed spike-detection algorithm and a simpler single threshold-crossing approach were tested to detect and analyze stimulation-induced responses.

2.5 Stimulation

To deliver stimulation patterns to the Intan head stages, two primary methods can be employed. The first is to send stimulation commands through the TCP Command Port. Testing revealed that the delays associated with this method due to transmission through the TCP Command Port, Intan RHX software, and the universal serial bus (USB) were inconsistent. To achieve consistent delays,

a second method was developed in which stimuli were digitally triggered through the I/Os of the Intan expansion box. This method required the use of an STM32F407 microcontroller, receiving stimulation commands through USB, with an onboard circular buffer implemented to compensate for any timing inconsistencies in data recording or software-based signal processing. The circular buffer allowed asynchronous data input and synchronous output, ensuring precise timing.

Prior to stimulation, the VWM software preprograms the stimulation parameters—including pulse shape, amplitude, pulse width, number of pulses, etc.—into the Intan controller. The stimulation trigger of each target electrode is assigned to a digital input signal on the Intan expansion box. The microcontroller generates these triggering pulses based on the commands received from the VWM software via USB in real time. Each rising edge of a pulse on the expansion box's digital input activated the preprogrammed stimulation on the corresponding electrode, with the expansion box relaying the stimulation triggers to the Intan controller. This entire synchronization process occurred within the firmware of the microcontroller and the Intan system, avoiding variability associated with operating systems and ensuring consistent timing. The final stimulation commands were transmitted to the headstages via Serial Peripheral Interface (SPI) cables.

Prior to running the VWM, a parameter optimization process was carried out to select the best stimulation parameters and target electrodes. This preliminary step ensured that the chosen parameters would robustly evoke post-stimulation activity while minimizing the risk of deleterious effects due to excessive or unbalanced charge density. A custom software tool called NeuroTuner was developed, interfacing with the Intan system via TCP. This tool facilitated systematic sweeps of stimulation across all electrodes on the MEA with different parameters, and data was recorded for offline analysis. The optimization process involved a symmetrical biphasic pulse sweep, starting with a current of 1 μA and a pulse width of 100 μs, which were systematically increased

to find the optimal combination. Our analysis identified a current of 10 µA with a pulse width of 500 µs for each phase as optimal, consistently generating adequate post-stimulation biological spikes while maintaining cell viability.

With the optimal parameters set, an electrode sweep was performed on each MEA by NeuroTuner to identify the most suitable target electrodes. The most effective electrodes were selected based on their higher neural activity levels post stimulus, physical distance from each other, and the presence of viable cells, as confirmed by microscopic imaging. On the other hand, source electrodes were selected based on noise RMS, spontaneous spike rate, and impedance. Electrodes with acceptable impedances (below 200 kΩ) were chosen, as higher impedance increases noise levels, often exceeding spike voltages, making spike detection impractical. The two electrodes with the lowest noise, highest spike activity, and acceptable impedance were chosen, ensuring independent and representative data collection. This careful selection process enhanced the reliability and quality of the recorded neural signals for analysis. Simultaneously, data from all 64 electrodes of the target MEA was recorded. Electrodes with impedance exceeding 200 kΩ or lacking significant activity post-stimulus were excluded from the analysis. This refinement resulted in 32 “active electrodes” being included for further analysis, enhancing the reliability and quality of the recorded neural signals.

To minimize stimulation-induced artifacts and amplifier railing—which occurs when stimulation voltages exceed the system's maximum readable voltage (6.4 mV for the Intan RHS system)—some neural recording devices offer blanking hardware features, namely the capability to completely turn off the amplifier and zero out the recording for a predefined time both pre- and post-stimulus to reduce artifacts caused by stimulation. However, this approach could potentially destabilize IIR filters due to DC-offset issues during the initiation phase following the zero-out

period. Since this feature is not available in the Intan system, an alternative method was employed to address these artifacts. The Intan system was configured to temporarily reduce the amplification gain across all electrodes of the stimulated head stage during the stimulation. While a low-pass filter (with Intan's default setting at 1000 Hz) is commonly used to filter out these high-frequency artifacts, it proved impractical because the initiation of the filter prior to stimulation introduced start-up artifacts, especially in the presence of residual DC voltage from previous stimulations. By

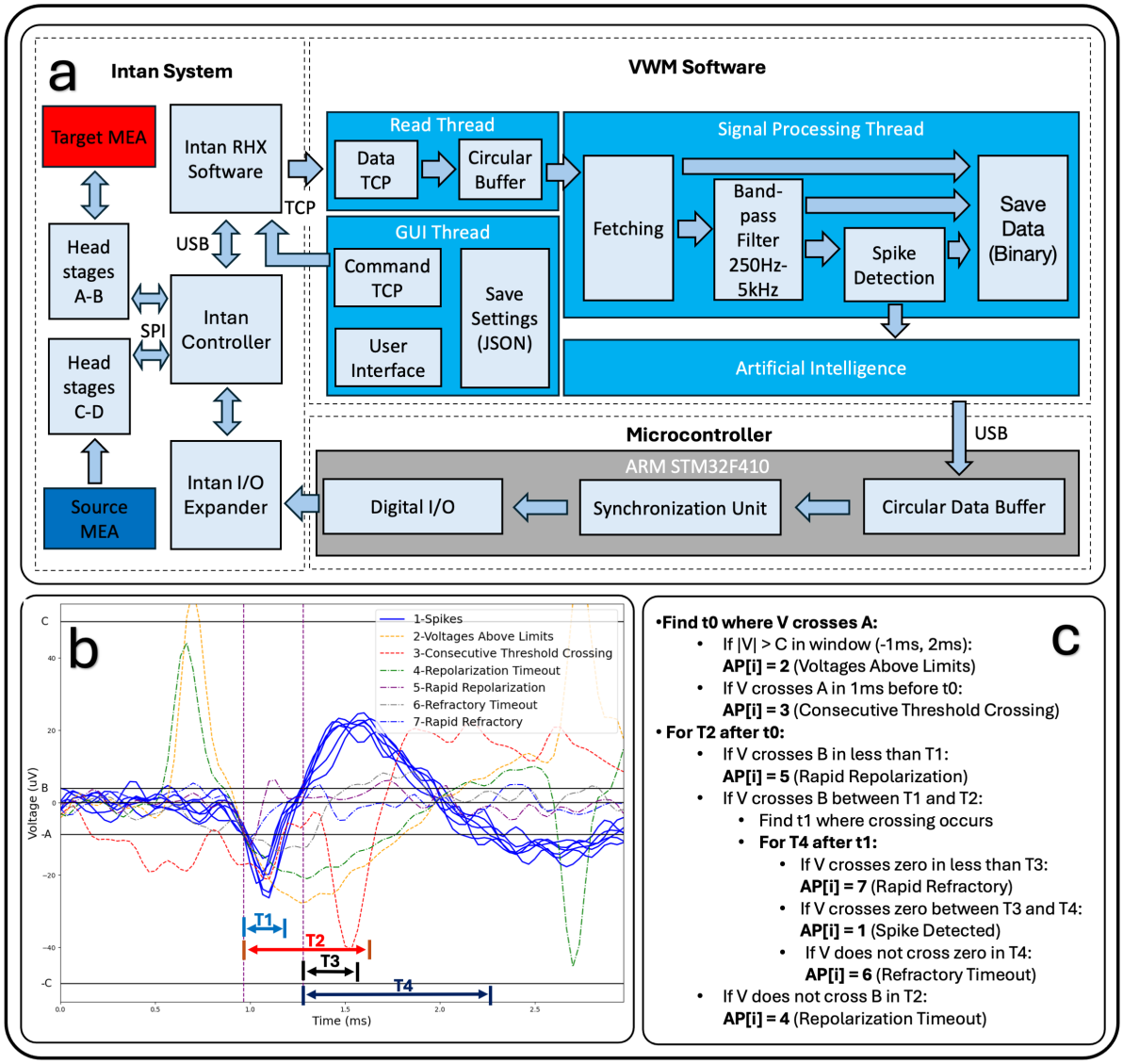

Figure 7: VWM and novel spike detection (a) Block diagram of the Virtual White Matter (VWM). (b) Examples of spike detection and artifact removal. (c) Pseudocode for spike detection.

instead reducing the amplification during stimulation, these issues were mitigated, leading to more accurate signal detection and reduced artifact impact [57]. The current controlled stimulation method has been employed for stimulations. Current-controlled stimulation offers several advantages over voltage-controlled stimulation in vitro experiments. One significant benefit is its ability to provide more precise and consistent control over the amount of current delivered to the target tissue. This precision helps minimize the risks of tissue damage that can arise from the unpredictable variations in tissue and electrode impedance, which can affect voltage-controlled systems. Due to the variations in the impedances of the electrodes, when stimulated through a voltage-controlled method, the amount of voltage delivered to the cell or tissue will not be the same for all the electrodes, making the results dependent on the electrode impedance. Additionally, current-controlled stimulation can achieve more uniform and reliable activation of neurons, which is crucial for the effectiveness of the experiments. This uniformity enhances the reproducibility of neural responses and can improve the overall outcomes of neuromodulation studies. The adaptability of current-controlled systems also facilitates more accurate dose-response relationships, enabling better customization of stimulation protocols to meet the experimental requirements [60,61].

2.6 Parameter Optimization

Optimizing stimulation parameters to evoke sufficient post-stimulation activity while preserving cell viability is critical to this project. Excessive stimulation currents can lead to cell depolarization or irreversible damage, while insufficient currents may fail to elicit significant neural activity. The key factor in effectively evoking cellular responses is the amount of charge delivered to the cells, measured in microcoulombs (μC), determined by the product of current and pulse width. To achieve this balance, we developed a software tool, NeuroTuner shown on Figure 8, which

interfaces with the Intan RHX Software via TCP. NeuroTuner enables precise configuration of stimulation paradigms and systematic electrode sweeps, as illustrated in Figure 8. Initial optimization involved symmetrical biphasic pulse sweeps with pulse widths ranging from 100 µs to 1000 µs and pulse amplitudes from 1 µA to 20 µA. Analysis identified a current of 10 µA with a pulse width of 500 µs as the optimal combination, consistently generating adequate post-stimulation spikes while maintaining cell viability.

With the optimal parameters set, an electrode sweep was performed on each MEA by NeuroTuner to identify the most suitable target electrodes. The most effective electrodes were selected based on their higher neural activity levels post stimulus, physical distance from each other, and the presence of viable cells, as confirmed by microscopic imaging. On the other hand, source

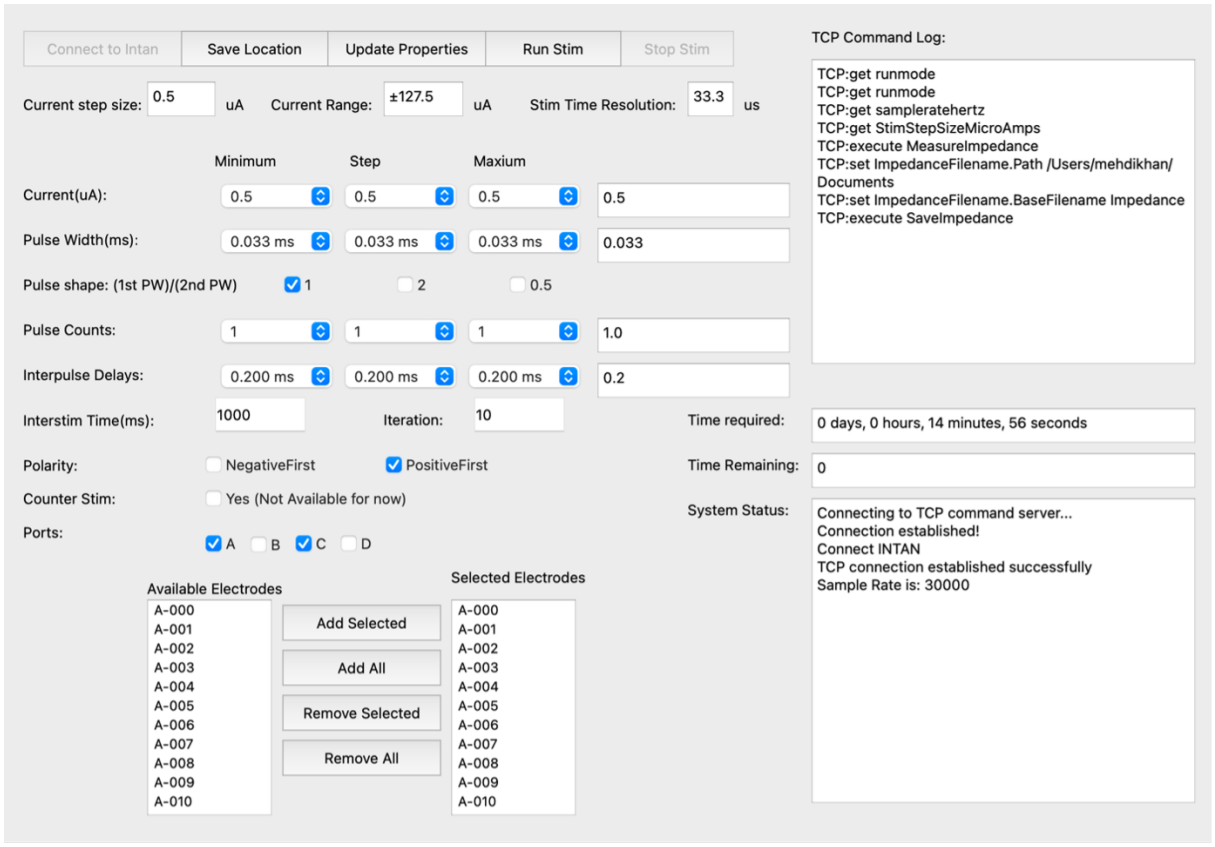

Figure 8: NeuroTuner Software to optimize electrical stimulation of neural preparations.

electrodes were selected based on noise RMS, spontaneous spike rate, and impedance. Electrodes with acceptable impedances (below 200 kΩ) were chosen, as higher impedance increases noise levels, often exceeding spike voltages, making spike detection impractical. The two electrodes with the lowest noise, highest spike activity, and acceptable impedance were chosen, ensuring independent and representative data collection. This careful selection process enhanced the reliability and quality of the recorded neural signals for analysis. Simultaneously, data from all 64 electrodes of the target MEA was recorded. Electrodes with impedance exceeding 200 kΩ or lacking significant activity post-stimulus were excluded from the analysis. This refinement resulted in 32 “active electrodes” being included for further analysis, enhancing the reliability and quality of the recorded neural signals.

3 Specific Aim 1

Aim 1: Develop a robust VWM platform for real-time cross-dish neural communication.

3.1 Description

The project's initial phase was to show the proof of the concept of the system and test its various functionalities. A simple forwarder system has been designed to detect the spikes from two source electrodes and stimulate two electrodes in the target dish. This initial design emulates interregional brain communication and serves as a basis for the future investigation of more sophisticated neural interactions.

Subsequently, we validated whether the detected spontaneous spikes and evoked responses were truly biological. This included applying MK-801 to block N-Methyl-D-aspartate (NMDA) receptor activity and confirm that the observed spikes were not due to noise or stimulation artifacts. We also tested the delay between spike detection and stimulation, which was set to 200 ms, and checked its consistency across trials.

To evaluate how well the system could distinguish between the two stimulation sites, we analyzed the post-stimulus spike activity across different electrodes in the target dish. We examined which time periods after stimulation contained the most useful information and found that the first 10 ms carried the strongest signal for classification. We also tested bidirectional communication, where each dish could send and receive signals from the other using the same 200 ms delay. This setup allowed us to observe feedback loops and test the system under more dynamic conditions, similar to real brain regions interacting.

3.2 Validation

To confirm that the spontaneous activity in the source dish and the stimulus-evoked activity in the target dish were biological, we used MK-801, an NMDA receptor channel blocker. The blocker

was applied to suppress neural activity and verify that the spikes observed before its introduction

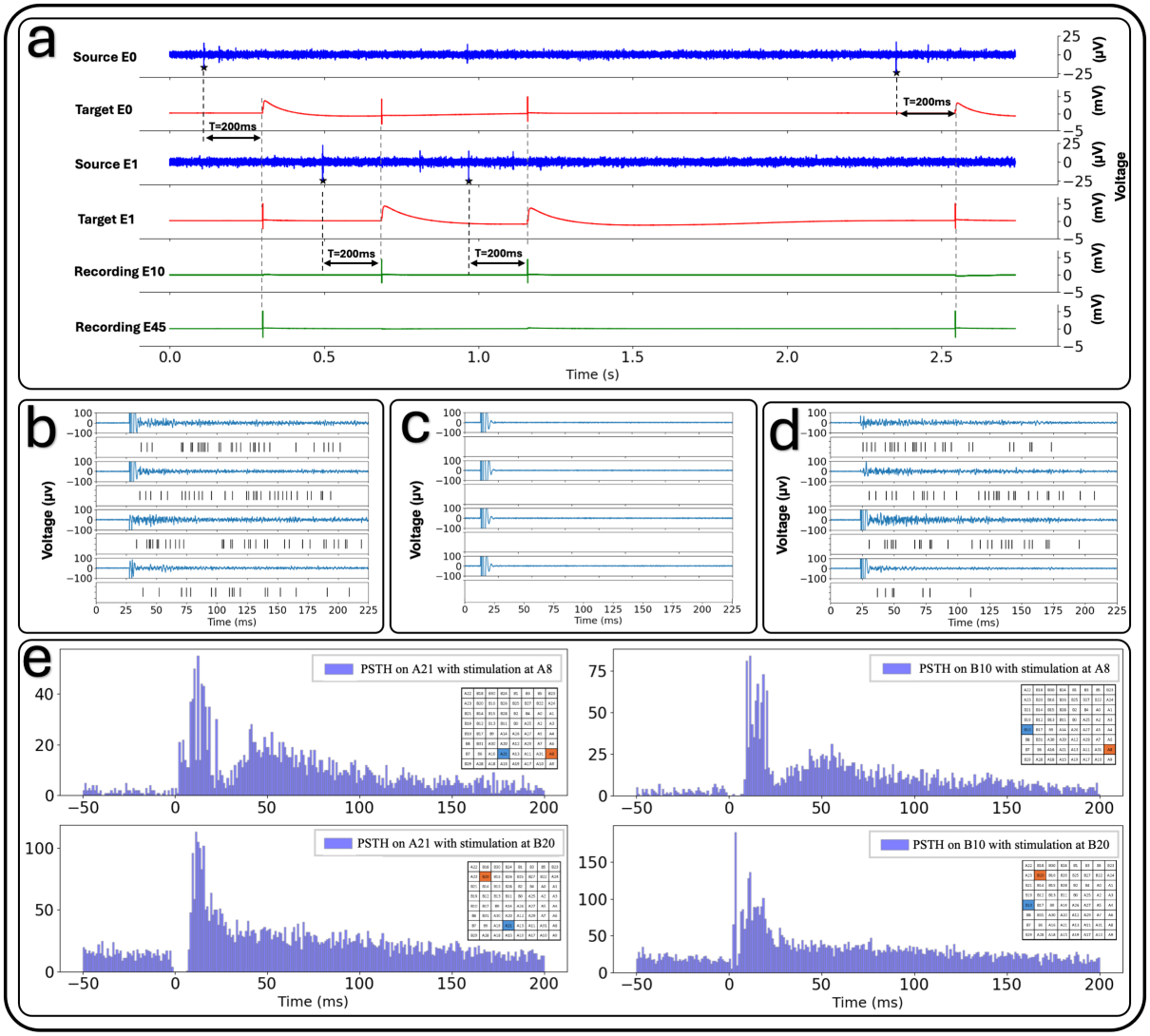

Figure 9: Initial results of the Vistual White Matter (VWM) test (a) Cross-sectional representation of spike detection, stimulation timing, and artifact propagation with recording electrodes in the VWM. (b) Post-stimulus high pass filtered activity showing spikes detected from recording electrodes on the target dish running the VWM, recorded before the application of any channel blockers. (c) Activity from recording electrodes on the target dish after the application of MK-801 to the target dish. (d) Activity from recording electrodes on the target dish after the removal of MK-801 from both dishes and subsequent cell recovery. (e) Post-Stimulus Time Histogram (PSTH) depicting responses from two electrodes (A21 on the left and B20 on the right) to stimulations delivered at target electrodes (0 above and 1 below). To minimize confounding effects of overlapping stimuli, only stimulations with no preceding events within 50 ms and no subsequent events within 200 ms were considered. Red markers denote the positions of the target electrodes, while blue markers indicate the positions of the recording electrodes on the MEA capturing the activity.

were indeed biological rather than noise or stimulation artifacts. MK801 selectively inhibits neural activity while preserving other conditions and signals, including noise and artifacts.

The blocker was administered to reach a final concentration of 85 μM in the media following data collection during the VWM experiments. Neural activity gradually diminished over the course of 30 minutes, eventually reaching a complete cessation. The VWM experiment was conducted to confirm that the neural activity detected in the source MEA represented true biological signals rather than noise. Afterward, the media was replaced, and the blocker was removed to allow recovery over 72 hours. Given MK801's reversible effects, a return of spontaneous activity was confirmed as expected, which indicated that the neural silence was due to the blocker and not from permanent cell damage, cell dislodgment from the MEAs, or other issues. The successful resumption of activity upon blocker removal confirmed the effect was indeed due to MK801. Furthermore, the same procedure was successfully implemented in the target dish to verify that stimulus-evoked neural activity was a true biological response rather than a stimulation artifact.

We evaluated the system's timing by analyzing delays between spike detection in the source dish and stimulation in the target dish, using data from the VWM experiments. After refining the spike detection algorithms and optimizing inter-thread and inter-system communication, we achieved consistent 200 ms delays from spike occurrence in the source dish to stimulation in the target dish. While the 200 ms delay can be adjusted, it was chosen based on typical neural processing times, such as reaction times to sensory stimuli (150-250 ms) [62] cortical processing in sensory pathways (100-200 ms) [63], and feedback loops in motor control (around 200 ms) [64], which are common in neural integration and response.

A key objective for evaluating the VWM was to assess how distinct the neural activity evoked by stimulation at each of the two target electrodes was by examining the stimulation responses across

various recording electrodes in the target dish. Given that stimulation in 2D MEAs can spread throughout the dish and potentially affect multiple regions similarly, it was important to evaluate the uniqueness of the evoked activity. We addressed this by analyzing Post-Stimulus Timing Histograms (PSTH) of detected spikes across different recording sites in the target dish, focusing on a 200 ms window following stimulation at each of the two target electrodes. This analysis helped determine the distinctiveness of the responses from the two stimulation sites.

We subsequently developed a machine learning model to classify the target electrode of delivered stimulations by analyzing spike timings from a combination of one or more active electrodes, with the two stimulus target electrodes as output labels. Spike times were binned in 1 ms intervals within a 200 ms window following each stimulation event, resulting in a matrix format compatible with machine learning for a VWM dataset spanning 26 minutes. To enhance computational efficiency and preserve data integrity, Principal Component Analysis (PCA) was applied to reduce dimensionality while retaining 95% of the variance (n_components = 0.95), and each binned feature was normalized using z-score normalization. To identify the most effective model for predicting the stimulated electrode in the source dish, using evoked responses from the target dish, we compared several machine learning algorithms, including K-Nearest Neighbor (KNN), Support Vector Machines (SVM), and Random Forests (RF). The dataset was split with 80% allocated for training and validation and the remaining 20% for testing.

To ensure a fair and unbiased evaluation of the model, we addressed two key sources of bias in our analysis. First, the dataset was unbalanced, with one target electrode having more stimulations than the other, which could potentially influence model performance. Second, relying solely on a simple train-test split risked introducing uneven data representation. To mitigate these issues, we employed stratified 10-fold cross-validation, which preserves class distribution in each fold and

ensures that the model is tested on a representative mix of data from both labels. We based our analysis on all data from the 32 identified active electrodes and subsequently evaluated various combinations of these electrodes to determine the optimal number of required electrodes to achieve satisfactory performance.

To address the presence of any unwanted stimulation artifacts, potentially erroneously detected as spikes, in our data, we applied both single-threshold and double-threshold algorithms for spike detection and tested the data from both methods using the same machine learning algorithms. For validation that responses were the products of biological activity (rather than artifactual), we used data from a target dish treated with the channel blocker MK-801, where stimulation occurred without any NMDA-mediated neural activity in the target dish. The analysis revealed that the double-threshold method effectively eliminated all artifacts from the feature set, whereas the single-threshold method allowed some artifacts to be present in the analysis. These findings demonstrate the effectiveness and robustness of our double threshold spike detection technique.

3.3 Results

The VWM system demonstrated the capability to create functional connections between distinct neural populations in separate MEA dishes by triggering precise stimulation based on detected spike activity. Key findings from the experiments are summarized as follows:

3.3.1 Spike Detection and Artifact Mitigation

Spike events satisfying the spike detection criteria were identified on source electrodes 0 and 1, triggering electrical stimulation on corresponding target electrodes with a consistent delay of 200 milliseconds. The temporal alignment between spikes and stimulations exhibited high consistency (Figure 9a). However, each stimulation generated artifacts on nearby electrodes, including those within the same head stage, the same dish, and even on adjacent dishes. The magnitude of these artifacts is influenced by factors such as electrode impedance, physical distance between

electrodes, and the design of the headstage chip and PCB traces. This can be seen in Figure 9a in the artifacts observed on the target electrodes as well as two randomly selected recording electrodes. When stimulation occurred on a headstage, a surge of electrical charge traveled through its SPI cable, creating a substantial electric field capable of interfering with nearby parallel cables. To mitigate this, we maintained at least 5 cm of separation between parallel cables. All recordings were conducted inside a grounded Faraday cage housed within a grounded incubator to minimize external electromagnetic noise.

3.3.2 Validation with MK-801

To validate the biological origin of recorded neural activity, the NMDA receptor antagonist MK-801 was employed. Prior to introducing MK-801, spontaneous activity in the source dish was consistently detected and used to trigger stimulation in the target dish, resulting in detectable stimulus-evoked neural responses (Figure 9b). Upon administering MK-801 to the source dish, spontaneous neural activity was suppressed, leading to the cessation of stimuli in the target dish. Washing out MK-801 restored neural activity in the source dish, which reactivated the whole system. When MK-801 was applied to the target dish, stimulation-evoked neural responses were effectively suppressed, despite the presence of external stimulation (Figure 9c). Removal of the antagonist from the target dish restored post-stimulus spike activity, confirming the system's capability to detect and utilize genuine neuronal interactions and thus verifying the biological nature of the recorded signals (Figure 9d).

3.3.3 Post-Stimulus Spike Time Histograms

To achieve the VWM's objective of transmitting information across dishes, it was critical to demonstrate that stimulation at two distinct target electrodes could evoke discriminable neural responses at other electrodes on the MEA. Given that stimulation in 2D MEAs can propagate and

influence multiple regions similarly, it was essential to assess whether the evoked activity post-stimulus was unique to each stimulation site. Demonstrating this uniqueness would confirm that information can be introduced into the neural preparation by stimulating distinct electrodes. Conversely, if stimulation at different electrodes produced identical post-stimulus neural activity, the ability to differentiate input sources would be compromised.

To assess the uniqueness of the evoked activity, we analyzed post-stimulus spike time histograms (PSTH) within a 200 ms window relative to each stimulation electrode. This comparative analysis allowed us to evaluate the distinctiveness of the neural responses elicited by each stimulation site. Figure 9e provides clear examples of the PSTH recorded from two different electrodes in response to stimulation at the two target electrodes. The PSTH plots demonstrate that the neural responses on the same electrode differ significantly depending on which target electrode was stimulated, confirming the ability to generate distinct neural activity patterns through stimulation of separate sites.

3.3.4 Artifact Removal

We tested the efficacy of single- and double-threshold spike detection methods for rejecting stimulus artifacts. Spikes detected from a combination of all active electrodes within 200 ms post-stimulus were used to train a machine learning algorithm to predict which of two electrodes had been stimulated. In the presence of MK-801, which silenced neural activity, the ML algorithms successfully differentiated between stimulus electrodes when trained with spikes detected using the single-threshold method. This indicates that, in the absence of biological activity, the stimuli were differentiable solely due to stimulation artifacts. In contrast, when trained using spikes detected with the double-threshold method under the same conditions, the differentiation between stimulus electrodes dropped to chance levels (accuracy around 0.5, Figure 10a).

These results underscore the importance of rejecting stimulation artifacts in BNN or VWM preparations, as artifacts otherwise can mistakenly masquerade as transmitted information. Based on these findings, subsequent analyses exclusively utilized data from the double-threshold method to ensure artifact-free results. Although the double-threshold technique effectively isolates genuine neural activity, it may occasionally miss certain biological events, such as closely occurring neuronal spikes that deviate from typical spike shapes. Despite this limitation, the developed double-threshold method reliably distinguishes target electrodes while significantly minimizing the influence of artifacts.

3.3.5 Machine Learning Analysis

After validating the spike detection methods, machine learning techniques were applied to data collected without the MK-801 blocker, where both biological activity and stimulation were present. The analysis focused on classifying target electrodes using spike data recorded during the first 200 ms post-stimulation, as shown in Figure 10b. Due to the combinatorial magnitude of analyzing all possible electrode combinations, random subsets of 100 combinations were generated and averaged for groups of 2, 3, 5, 10, 15, 20, 25, and 30 electrodes. For scenarios involving either a single electrode or all 32 active electrodes, the full set of possible combinations was evaluated, resulting in 32 and 1 combination(s), respectively. This approach ensured a balance between computational efficiency and analytical rigor, providing insights into how electrode numbers and selection affect classification performance. The findings highlight the relationship between the number of electrodes used and the overall accuracy of the machine learning model.

To determine which electrodes and time frames provided the most valuable information for classifying stimulation targets, three metrics were applied: information gain, chi-square tests, and

Fisher's score. These analyses, shown in Figure 10c, identified the channels and time frames most

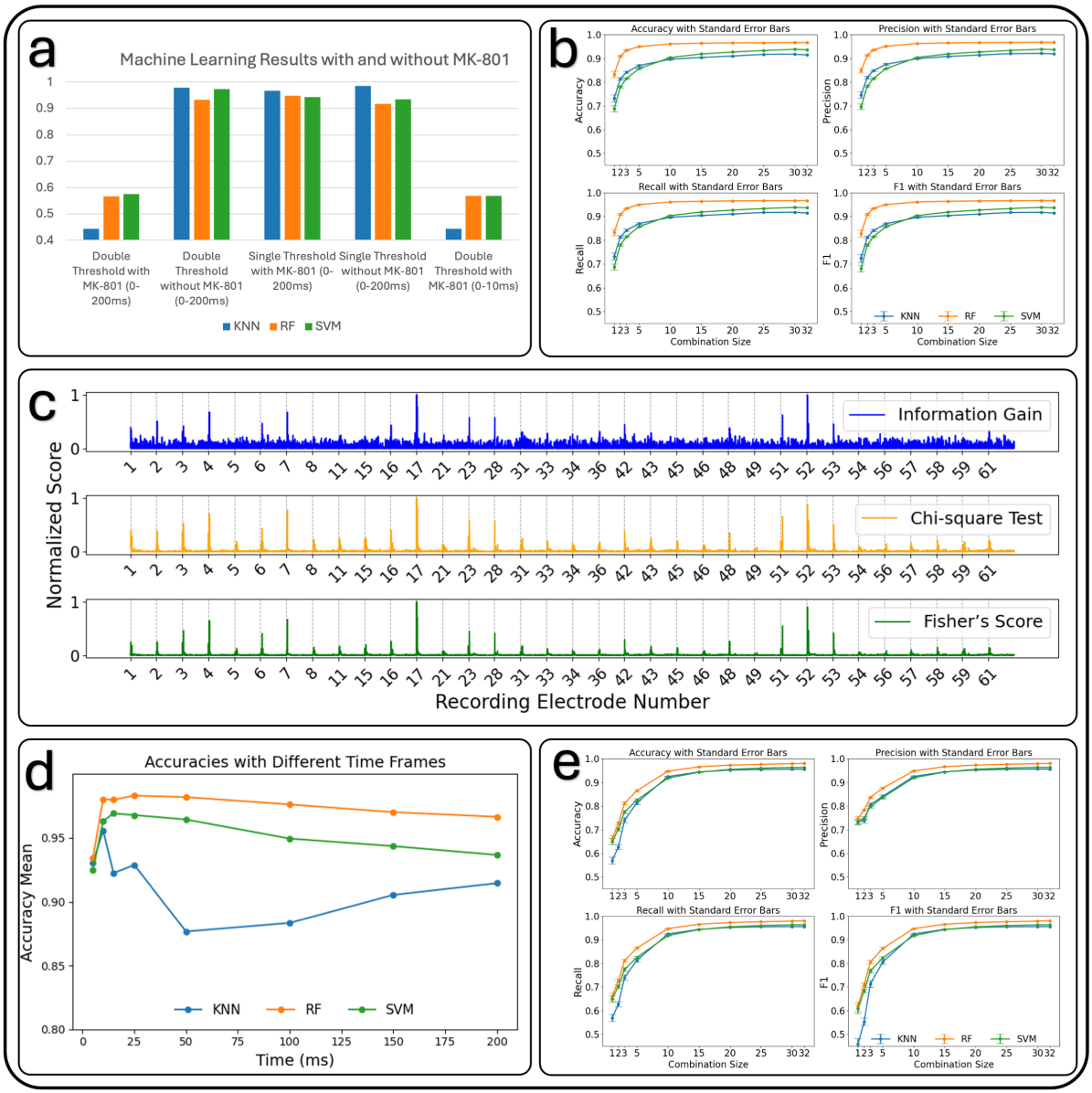

Figure 10: Illustration of mono-directional VWM-1 and results of the experiment. ***(a)*** *Comparison of machine learning performance for spike detection using single and double threshold methods, analyzed with and without the application of MK-801 to the target dish.* ***(b)*** *Machine learning classification results utilizing various electrode combinations, analyzing 200 ms of post-stimulus neural data. Models include Random Forest (RF), Support Vector Machine (SVM), and K-Nearest Neighbors (KNN).* ***(c)*** *Normalized scores representing the information richness of individual electrodes over different post-stimulus time points, highlighting their contribution to classification performance.* ***(d)*** *Accuracy of machine learning models employing data from all active electrodes, evaluated across varying post-stimulus time windows.* ***(e)*** *Machine learning results comparing different electrode combinations using 10 ms of post-stimulus neural data.*

critical for machine learning classification. In Figure 10c, each section of the x-axis represents the 200 ms post-stimulus window for the specified active electrode, and the y-axis reflects the importance scores assigned to each time point for each electrode. Notably, the large spikes at electrodes 17 and 52 indicate the special relevance of these two electrodes for decoding the source electrode.

Additionally, the peaks consistently occur within the first 10 ms of the post-stimulus window, highlighting the significance of this early time frame for classification and led to an investigation of how performance changes when using only specific portions of the early post-stimulation data. Various time frames, starting with the first few milliseconds after stimulation, were analyzed using data from all active electrodes. As shown in Figure 10d, optimal performance was achieved when focusing on the first 10 ms of spike activity post-stimulation. Extending the analysis to longer time frames resulted in a decrease in accuracy, likely due to burst activity. During bursts, a large proportion of neurons synchronize their activity, which may confound the machine learning algorithms and obscure the differentiation between stimulation sources.

Additionally, Figure 10e illustrates the relationship between the number of electrodes used and classification accuracy for the 10 ms time frame. While the first 10 ms contained the most valuable information, reducing the number of electrodes also led to a decrease in accuracy, likely due to the smaller dataset available for training. Conversely, using more electrodes improved classification performance but with diminishing returns beyond a certain number of electrodes. These findings highlight the importance of early neural responses and comprehensive electrode coverage for accurate classification, providing insights into optimizing data collection and processing for future studies. Furthermore, we applied the same machine learning approach to data combined from all electrodes under MK-801 conditions in the target dish, using a doubled threshold within the 0–10

ms period. As shown in Figure 10a, even focusing solely on the first 10 ms did not enhance accuracy when MK-801 was present. This outcome suggests that the improvements observed in other conditions are driven primarily by biological neural activity rather than stimulation artifacts. Overall, the machine learning results demonstrate that using a traditional window discriminator double-threshold approach and 10 ms windows post-stimulus enables the system to introduce information into a neural preparation and extract information processed by the BNN. This neural processing holds immense value as it can be leveraged for diverse applications, such as image processing, signal filtering, and other tasks where BNNs can interpret and relay information between neural systems.

3.3.6 Bidirectional Connection:

A key feature of the VWM platform is its ability to establish real-time bidirectional communication between two independent neural cultures on separate MEAs as shown in Figure 11a This capability allows the system to model the reciprocal interregional communication observed in biological neural circuits, where most brain regions are interconnected in a bidirectional manner. In the current proof-of-concept implementation, spikes detected from either MEA trigger stimulation on the other MEA after the same fixed delay of 200 ms. Each MEA includes two dedicated electrodes for spike detection and two separate electrodes for stimulation. The same spike detection algorithm is applied symmetrically to both networks, enabling fully reciprocal closed-loop interactions without any gating or filtering of the stimulation events.

This unrestricted bidirectional configuration was designed to explore emergent network dynamics and information flow between dissociated neural populations. However, one observed consequence is the formation of positive feedback loops, where stimulation on one MEA evokes activity that subsequently triggers stimulation on the other MEA, potentially resulting in self-

sustained excitatory activity. These feedback loops can lead to excessive stimulation, which in turn induces a temporary reduction in neural activity due to depolarization block—a phenomenon in which prolonged or intense stimulation inhibits neuronal firing temporarily [65,66]. Notably, this

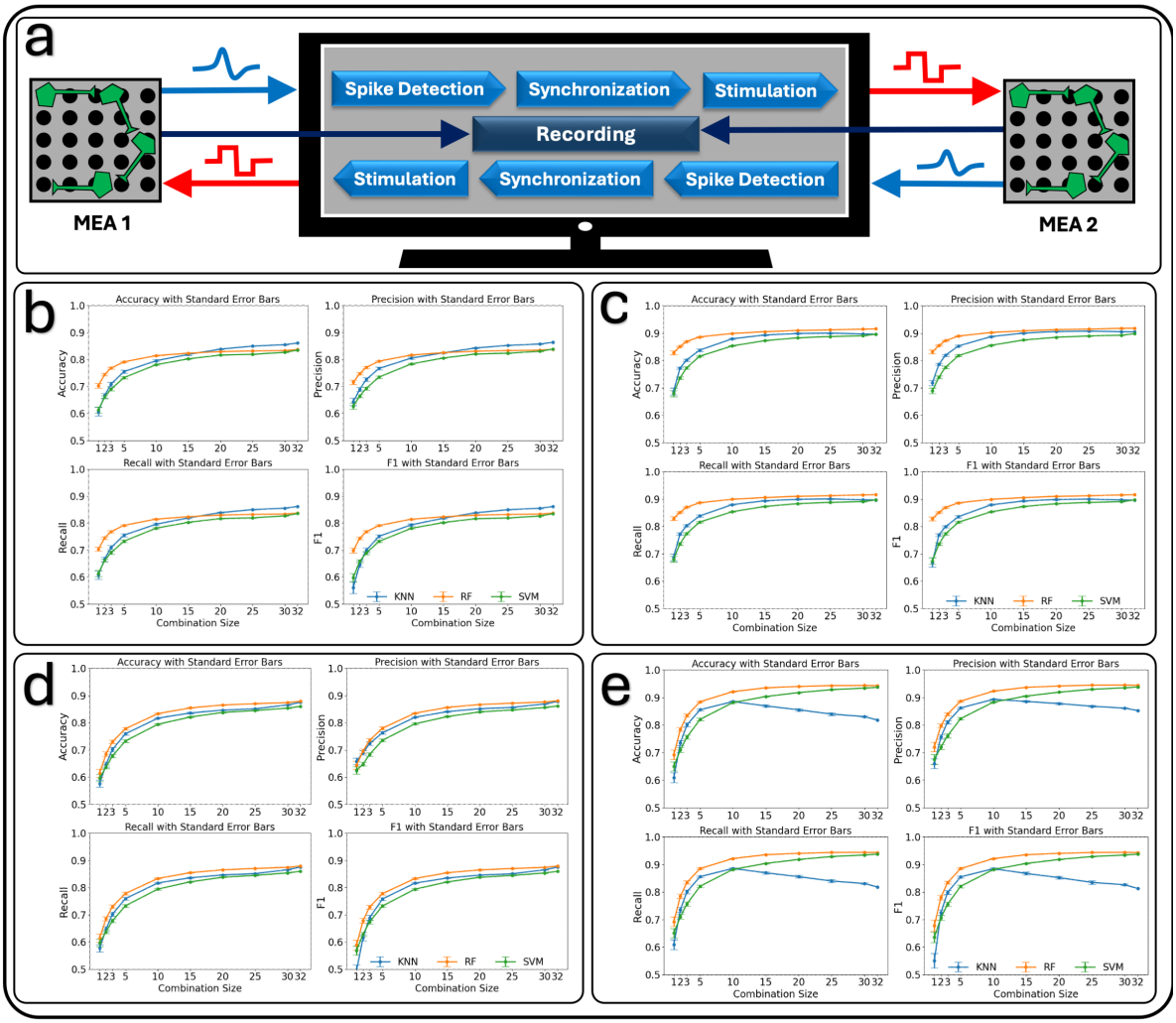

Figure 11: Illustration of bidirectional bi-directional VWM-1 and results of the experiment. (a) Schematic representation of the bidirectional Virtual White Matter (VWM) configuration. Spikes detected on one Micro Electrode Array (MEA) trigger stimulation on the opposite MEA after a fixed 200 ms delay, allowing reciprocal communication between two dissociated neural networks. (b) Classification results for MEA1, and (c) Classification results for MEA2, based on 200 ms post-stimulus activity from 32 selected electrodes in the bidirectional VWM setup. (d) Classification results for MEA1, and (e) Classification results for MEA2, based on 10 ms post-stimulus activity from 32 selected electrodes in the bidirectional VWM setup.

suppression is reversible, with spontaneous activity typically resuming a few seconds after stimulation ceases.

To evaluate the system's classification performance under bidirectional conditions, machine learning models were trained independently for each MEA using post-stimulus activity from 32 selected electrodes over a recording duration of 12 minutes. Results for the 200 ms analysis window are shown in Figure 11b for MEA1 and Figure 11c for , while results for the 10 ms analysis window are presented in Figure 11d and Figure 11e, respectively. Overall performance was slightly lower compared to the unidirectional configuration, likely due to overlapping stimulation events caused by positive feedback loops. These overlaps within the analysis window obscured distinct evoked response patterns, diminishing the models' ability to accurately classify the stimulation source. However, similar to the unidirectional VWM, the 10 ms post-stimulus data yielded slightly better results than the 200 ms data, as shorter windows reduced the likelihood of additional overlapping stimulations.

4 Specific Aim 2

In the second phase of the VWM experiment, as shown in Figure 12, spontaneous neural activity on the source MEA will be replaced with coded information. Two electrodes are used as binary markers representing “0” and “1,” enabling the transmission of structured data such as letters, numbers, or Morse code. We use a 3-bit coding scheme (8 possible codes). For each code, the corresponding stimulation is delivered through these electrodes with an inter-bit time interval of 1 second. This delay was selected for the initial experiments to allow the network to return to a stable, non-bursting state between stimulations. Evoked neural activity is recorded from the remaining electrodes within a fixed post-stimulation window (e.g., 10–200 ms, segmented into 1 ms bins). During later stages of the experiment, different inter-bit intervals will be tested to determine the minimum required delay for reliable information transmission.

The recorded, binned spike data is then processed by a machine learning system to decode the original 3-bit input. The recovered code is transmitted to a second MEA by stimulating two of its electrodes and a second machine learning system decodes the evoked response from the second MEA, establishing a one-way VWM connection. In the next step, the decoded code is sent back from the second MEA to the first, completing a bidirectional communication loop. This setup requires four distinct machine learning models—two for each direction.

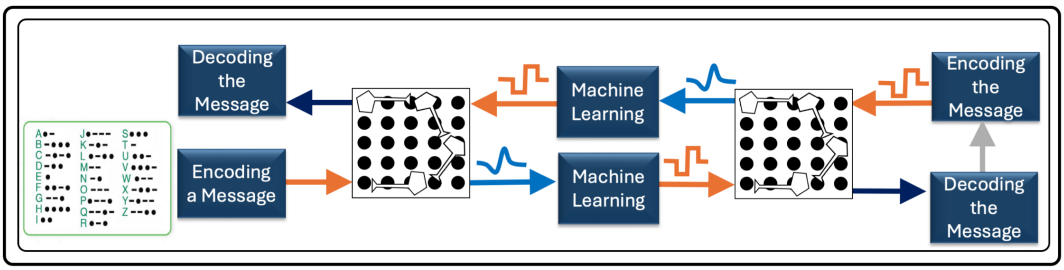

Figure 12: Illustration of bidirectional VWM-2. Information transmission and reconstruction happens between two interconnected Biological Neural Networks (BNNs) via Virtual White Matter (VWM).

This experiment evaluates all 8 combinations of a 3-bit code and aims to identify parameters including: (1) the maximum decoding accuracy of the machine learning models in unidirectional (2 models) and bidirectional (4 models) modes, (2) the overall accuracy of transmitting a full 3-bit message in both modes, (3) the minimum required interval between each bit, (4) the shortest effective post-stimulation time window for accurate decoding, and (5) the minimum time needed to transmit a complete 3-bit message. These tests will be conducted using three different MEA sets, each evaluated at two distinct time points corresponding to specific days in vitro (DIV).

Next, we investigate the possibility of removing the machine learning inference stage between the two MEAs and instead directly stimulating the second MEA using the binned spike data from the first MEA. Based on the results from the initial VWM phase (Figure 10b and e), we know that a trained machine learning model can identify the source of stimulation with over 80% accuracy using combined binned spike data from five electrodes within a 10 or 200 ms time window. Building on this, we will select the six best-performing electrodes and use their binned spike activity to construct a new stimulation pattern. This pattern will be delivered to the second MEA via two designated stimulation electrodes. The binned data from half of the selected electrodes will

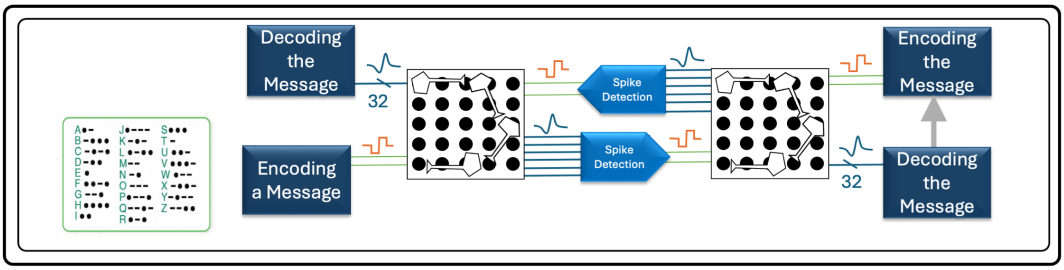

Figure 13: Diagram of the final step. After MEA1 is stimulated by the encoded message, spike data from six key electrodes (recorded in 10–200 ms bins) is used to drive MEA2's BNN, which propagates this input across its electrode array. The resulting spikes are then detected, binned, and used to reconstruct the original code—proving data can travel between MEAs without direct decoding. For a bidirectional link, the recovered code from MEA2 is re-encoded as bits on two electrodes and sent back to MEA1.

be time-combined and used to stimulate one electrode, while the remaining half will be used for the second. Six electrodes were chosen instead of five to both increase the accuracy and allow an even split for constructing the two stimulation signals.

In this setup, no machine learning is used between the two MEAs. Instead, we allow the BNN in the second MEA to interpret the incoming pattern. The evoked activity in the second MEA will then be recorded, binned, and passed through a machine learning model to reconstruct the original code. As illustrated in Figure 13, this test explores whether meaningful information can be transmitted from one MEA to another—through biological processing alone—without intermediate digital decoding.

To establish a bidirectional system, the recovered code from the second MEA will be re-encoded and sent back to the first MEA using the same stimulation method. The final decoded result from the first MEA will be compared with the original input. With 8 possible 3-bit codes, chance-level accuracy is 12.5% (1/8). Consistently higher accuracy across multiple trials would confirm successful information transmission via VWM without intermediate machine learning. All previously measured parameters—including decoding accuracy, required minimum post-stimulus time windows, required minimum inter-bit timing, and minimum total transmission duration—will also be evaluated in this experiment.

5 Conclusion

In vitro cell culture systems of the mammalian nervous systems are inherently limited since they cannot recapitulate the complex circuitry and can only sustain fragments. VWM opens the door to reconstructing circuits across a scalable number of specimens, and to investigating the effects of what removing and adding specimens might do to the physiological properties of the assembly. While individual specimens may have limited longevity, when multiple specimens are linked together by VWM, it could allow specimens that have deteriorated to be swapped out while maintaining the global integrity of the assembled hybrid system. The hardware framework described here is agnostic as to the type of specimens (dissociated, aggregates, organotypic slices, organoids) and to whether the specimens are in vitro or in vivo. The ability to reciprocally link in vivo neural activity to in vitro neural activity could enable exploration of novel substrate expansion, whereby the brain of a living organism would have additional neural substrate, even if ultimately the auxiliary neural tissue were implanted. The VWM platform allows characterization each given specimen as a transfer function [67]. The VWM platform also allows investigators to interpose in silico models (whether traditional machine learning artificial neural networks, or neuromorphic firmware) between neural specimens to see how the hybrid assembly performs. VWM in vitro can be thought of as the fundamental counterpart to BCIs that implants tens to tens of thousands of channels for stimulation and recording: namely, rather than implanting numerous sensor/recording elements into a living brain, VWM opens the door of rebuilding a brain around those elements.

Future enhancements will further validate and extend the system's capabilities. Incorporating additional MEAs, including high-density MEAs or 3D MEAs, will increase the resolution for recording and stimulation, supporting more detailed studies of neural dynamics. Developing

portable systems capable of controlling environmental parameters such as temperature and CO_2 levels, while also automating media exchange, will enable the long-term viability of brain slices without human intervention. These advancements are critical for sustaining neural preparations for weeks and exploring more complex neural dynamics. Such systems could also find applications in pharmacological studies by enabling the integration of drug delivery systems to evaluate how various compounds influence interconnected neural preparations. Additionally, the platform could be used to model neural disorders, such as epilepsy, Parkinson's disease, and Alzheimer's disease, in a controlled and reproducible environment.

An exciting avenue for enhancement lies in enabling closed-loop real-time operation. By recording and processing activity from interconnected neural preparations and delivering stimulation based on this activity, the system can replicate neural networks similar to those observed in living organisms, such as the interaction between the lateral geniculate nucleus (LGN) and the visual cortex. Incorporating real-time machine learning models into this closed-loop system will enable the identification of well-known neural patterns and the dynamic optimization of stimulation protocols. This approach, supported by artificial intelligence (AI), allows for the design of preplanned stimulation scenarios tailored to specific experimental needs. The use of diverse stimulation patterns, including variations in pulse shapes, widths, currents, frequencies, and numbers, will evoke a broader range of neural activity, making the system suitable for investigating complex neural processes.

Another critical improvement involves transitioning the system from software-based computer implementations to embedded platforms, such as FPGAs or microcontrollers, to reduce latency between spike detection and stimulation. This shift will significantly enhance the system's real-time processing capabilities, ensuring more accurate and immediate responses. Furthermore, the

integration of the system into a global network via the internet—the "Internet of Neurons" (IoN)—will enable interconnected neural preparations across laboratories, cities, or even continents. Such a globally distributed network would facilitate collaborative experiments on an unprecedented scale, advancing the field of neuroscience.

By enabling the creation of assemblies of two or more specimens, VWM could also open the door to virtual embodiment of more complex virtual organisms. Whereas motor and sensory assembloids allow for pathway reconstruction in a single dish [68], VWM could enable an assembly of assembloids (or other specimen types) that could then be embodied as an entity navigating a virtual, simulated world. We predict that the more the assembly system recapitulates the complexity of the nervous systems of intact animals, the more likely the emergent system will be to navigate more complex environments, and to move beyond the relatively constrained environments of Pong or solving a maze, towards more naturalistic scenarios of survival and exploration. These hybrid systems could also serve as more valid models for disease processes and screening therapeutics.

Additional enhancements could expand the system's functionality by incorporating multisensory inputs, such as optical, chemical, or mechanical signals, alongside electrical signals. Combining optogenetic stimulation with electrical recording would allow for precise spatiotemporal control over specific neural circuits or cell types, such as those in the retina. This integration would enable the system to process image information and interconnect it with BNNs for further processing. By simulating comprehensive neural processing scenarios, the system could bridge the gap between artificial and biological networks.

The system also holds potential for BCI applications, particularly by linking in vitro and in vivo neural systems to human neural systems. Such advancements could pave the way for creating

auxiliary neural substrates for therapeutic or enhancement purposes. The development of autonomous protocol optimization systems, driven by AI, will further streamline experimental processes by dynamically adjusting experimental parameters based on real-time results. This capability is essential for efficiently exploring the vast parameter space involved in neural stimulation studies.

This study presents VWM, a novel platform that enables real-time functional connectivity between neural cultures in separate multi-electrode array (MEA) dishes, bridging the gap between single-dish in vitro models and the complex interregional dynamics of BNNs. By replicating interregional communication and facilitating controlled interactions between heterogeneous cultures, VWM opens new opportunities to investigate neural coding, plasticity, and dynamic network behaviors. The system provides a robust and flexible platform for pharmacological testing, disease modeling, and the creation of sophisticated BNNs. By integrating machine learning, AI-driven optimization, and global connectivity, VWM advances biocomputing and hybrid systems while paving the way for next-generation brain-computer interfaces. These innovations offer transformative tools for neuroscience research and translational applications, laying the foundation for new frontiers in understanding and harnessing neural processing.

6 Timeline

MEA Plating & Usage Plan (April–August 2025):

Plating Date	Usable Window (DIV 14–35)	Purpose
April 9	April 23 – May 5	First round of experiments (Fig. 12)
April 30	May 14 – May 28	Continued Fig. 12 + ML training
May 21	June 4 – June 25	Fig. 13 BNN-based testing
June 11	June 25 – July 16	Repetition of Fig. 12 and Fig. 13
July 2	July 16 – August 6	Redundant ML training, long-term data
July 23	August 6 – August 27	Final testing and manuscript figures
August 13	August 27 – September 17	Backup MEAs or extended data recording
September 3	September 17 – October 8	Final experimental, replication, and refinement

Machine Learning, Thesis, and Manuscript Timeline (May–December 2025):

In **May 2025**, the primary focus will be on launching the first phase of experiments described in Figure 12. These experiments involve encoding 3-bit binary codes and decoding them using machine learning. Four machine learning models—two for each transmission direction—will be trained. Initial data will be collected to assess decoding accuracy, post-stimulation time windows, and inter-bit intervals.

In **June and July 2025**, the second phase of experiments, detailed in Figure 13, will begin. This phase tests the ability of biological neural networks to interpret stimulation patterns without any machine learning in the transmission pathway. Stimulation patterns will be derived from binned

spike data and delivered directly to a second MEA. However, machine learning will still be used for decoding at the receiving end. Data will continue to be collected across multiple MEAs to improve generalizability and reliability.

In **August and September 2025**, experiments for both phases will continue. Focus will be placed on redundant testing with different MEA batches, long-term comparisons across days in vitro, and exploring variations in stimulation patterns, electrode selection, and decoding windows. Final validation experiments will also be conducted to evaluate system robustness and to identify the best-performing configurations for communication.

From **October through December 2025**, the emphasis will shift entirely to writing and final analysis. The second manuscript will be written and revised for journal submission, with finalized figures, statistical results, and discussion. In parallel, the PhD thesis will be developed to include comprehensive coverage of all experimental phases, key findings, and future directions. Both the thesis and manuscript are expected to be finalized and submitted by the end of **December 2025**.

7 References

1. Napoli A, Obeid I. Investigating brain functional evolution and plasticity using microelectrode array technology. Brain Research Bulletin. 2015;119:127–35.

2. Massobrio P, Tessadori J, Chiappalone M, Ghirardi M. In vitro studies of neuronal networks and synaptic plasticity in invertebrates and in mammals using multielectrode arrays. Neural Plast. 2015;2015:196195.

3. Napoli A, Xie J, Obeid I. Understanding the temporal evolution of neuronal connectivity in cultured networks using statistical analysis. BMC Neuroscience. 2014 Jan;15[1]:17.

4. Kagan BJ, Kitchen AC, Tran NT, Habibollahi F, Khajehnejad M, Parker BJ, et al. In vitro neurons learn and exhibit sentience when embodied in a simulated game-world. Neuron. 2022 Dec 7;110[23]:3952-3969.e8.

5. Bisio M, Pimashkin A, Buccelli S, Tessadori J, Semprini M, Levi T, et al. Closed-Loop Systems and In Vitro Neuronal Cultures: Overview and Applications. In: Chiappalone M, Pasquale V, Frega M, editors. In Vitro Neuronal Networks: From Culturing Methods to Neuro-Technological Applications [Internet]. Cham: Springer International Publishing; 2019 [cited 2024 Aug 28]. p. 351–87. Available from: https://doi.org/10.1007/978-3-030-11135-9_15

6. Eytan D, Brenner N, Marom S. Selective adaptation in networks of cortical neurons. J Neurosci. 2003 Oct 15;23[28]:9349–56.

7. le Feber J, Stegenga J, Rutten WLC. The effect of slow electrical stimuli to achieve learning in cultured networks of rat cortical neurons. PLoS One. 2010 Jan 25;5[1]:e8871.

8. Shahaf G, Marom S. Learning in networks of cortical neurons. J Neurosci. 2001 Nov 15;21[22]:8782–8.

9. DeMarse TB, Wagenaar DA, Blau AW, Potter SM. The Neurally Controlled Animat: Biological Brains Acting with Simulated Bodies. Autonomous Robots. 2001 Nov 1;11[3]:305–10.

10. Ruaro ME, Bonifazi P, Torre V. Toward the neurocomputer: image processing and pattern recognition with neuronal cultures. IEEE Trans Biomed Eng. 2005 Mar;52[3]:371–83.

11. Feinerman O, Rotem A, Moses E. Reliable neuronal logic devices from patterned hippocampal cultures. Nature Phys. 2008 Dec;4[12]:967–73.

12. Bakkum DJ, Chao ZC, Potter SM. Spatio-temporal electrical stimuli shape behavior of an embodied cortical network in a goal-directed learning task. J Neural Eng. 2008 Aug;5[3]:310.

13. Novellino A, D'Angelo P, Cozzi L, Chiappalone M, Sanguineti V, Martinoia S. Connecting Neurons to a Mobile Robot: An In Vitro Bidirectional Neural Interface. Comput Intell Neurosci. 2007;2007:12725.

14. Warwick K, Xydas D, Nasuto S, Becerra V, Hammond M, Downes J, et al. Controlling a Mobile Robot with a Biological Brain. Defence Science Journal. 2010 Jan 30;60:5–14.

15. Reger BD, Fleming KM, Sanguineti V, Alford S, Mussa-Ivaldi FA. Connecting brains to robots: an artificial body for studying the computational properties of neural tissues. Artif Life. 2000;6[4]:307–24.

16. DeMarse TB, Dockendorf KP. Adaptive flight control with living neuronal networks on microelectrode arrays. In: Proceedings 2005 IEEE International Joint Conference on Neural Networks, 2005 [Internet]. Montreal, QC, Canada: IEEE; 2005 [cited 2024 Aug 28]. p. 1548–51. Available from: http://ieeexplore.ieee.org/document/1556108/

17. Cai H, Ao Z, Tian C, Wu Z, Liu H, Tchieu J, et al. Brain organoid reservoir computing for artificial intelligence. Nat Electron. 2023 Dec;6[12]:1032–9.

18. Sumi T, Yamamoto H, Katori Y, Moriya S, Konno T, Sato S, et al. Biological neurons act as generalization filters in reservoir computing. Proc Natl Acad Sci USA. 2023 Jun 20;120[25]:e2217008120.

19. Berger TW, Ahuja A, Courellis SH, Deadwyler SA, Erinjippurath G, Gerhardt GA, et al. Restoring lost cognitive function. IEEE Eng Med Biol Mag. 2005;24[5]:30–44.

20. DeMare L. Wetware: A Computer in Every Living Cell. Yale J Biol Med. 2011 Jun;84[2]:174–5.

21. Jordan FD, Kutter M, Comby JM, Brozzi F, Kurtys E. Open and remotely accessible Neuroplatform for research in wetware computing. Front Artif Intell. 2024 May 2;7:1376042.

22. Smirnova L. Biocomputing with organoid intelligence. Nat Rev Bioeng. 2024 Aug;2[8]:633–4.

23. Smirnova L, Caffo BS, Gracias DH, Huang Q, Morales Pantoja IE, Tang B, et al. Organoid intelligence (OI): the new frontier in biocomputing and intelligence-in-a-dish. Front Sci [Internet]. 2023 Feb 28 [cited 2024 Aug 19];1. Available from: https://www.frontiersin.org/journals/science/articles/10.3389/fsci.2023.1017235/full

24. Goñi-Moreno A, Nikel PI. High-Performance Biocomputing in Synthetic Biology–Integrated Transcriptional and Metabolic Circuits. Front Bioeng Biotechnol [Internet]. 2019 Mar 11 [cited 2024 Aug 28];7. Available from: https://www.frontiersin.org/journals/bioengineering-and-biotechnology/articles/10.3389/fbioe.2019.00040/full

25. Vallejo-Mancero B, Faci-Lázaro S, Zapata M, Soriano J, Madrenas J. Real-time hardware emulation of neural cultures: A comparative study of in vitro, in silico and in duris silico models. Neural Networks. 2024 Nov 1;179:106593.

26. Mariana M, Roque C, Baltazar G, Cairrao E. In Vitro Model for Ischemic Stroke: Functional Analysis of Vascular Smooth Muscle Cells. Cell Mol Neurobiol. 2022 Oct 1;42[7]:2289–304.

27. Van Breedam E, Ponsaerts P. Promising Strategies for the Development of Advanced In Vitro Models with High Predictive Power in Ischaemic Stroke Research. International Journal of Molecular Sciences. 2022 Jan;23[13]:7140.

28. Chiappalone M, Cota VR, Carè M, Di Florio M, Beaubois R, Buccelli S, et al. Neuromorphic-Based Neuroprostheses for Brain Rewiring: State-of-the-Art and Perspectives in Neuroengineering. Brain Sci. 2022 Nov 19;12[11]:1578.

29. Shupe LE, Miles FP, Jones G, Yun R, Mishler J, Rembado I, et al. Neurochip3: An Autonomous Multichannel Bidirectional Brain-Computer Interface for Closed-Loop Activity-Dependent

Stimulation. Front Neurosci [Internet]. 2021 Aug 19 [cited 2024 Aug 19];15. Available from: https://www.frontiersin.org/journals/neuroscience/articles/10.3389/fnins.2021.718465/full

30. Cannon SC. Pathomechanisms in channelopathies of skeletal muscle and brain. Annu Rev Neurosci. 2006;29:387–415.

31. Kullmann DM, Waxman SG. Neurological channelopathies: new insights into disease mechanisms and ion channel function. J Physiol. 2010 Jun 1;588[Pt 11]:1823–7.

32. Yizhar O, Fenno LE, Prigge M, Schneider F, Davidson TJ, O'Shea DJ, et al. Neocortical excitation/inhibition balance in information processing and social dysfunction. Nature. 2011 Sep;477[7363]:171–8.

33. Cui H, Xie X, Xu S, Chan LLH, Hu Y. Electrochemical characteristics of microelectrode designed for electrical stimulation. BioMedical Engineering OnLine. 2019 Aug 1;18[1]:86.

34. Holt GR, Koch C. Electrical Interactions via the Extracellular Potential Near Cell Bodies. J Comput Neurosci. 1999 Mar 1;6[2]:169–84.

35. Quiroga RQ, Nadasdy Z, Ben-Shaul Y. Unsupervised spike detection and sorting with wavelets and superparamagnetic clustering. Neural Comput. 2004 Aug;16[8]:1661–87.

36. Lewicki MS. A review of methods for spike sorting: the detection and classification of neural action potentials. Network: Computation in Neural Systems. 1998 Jan;9[4]:R53–78.

37. Erofeev A, Antifeev I, Bolshakova A, Bezprozvanny I, Vlasova O. In Vivo Penetrating Microelectrodes for Brain Electrophysiology. Sensors (Basel). 2022 Nov 23;22[23]:9085.

38. Utah Array, Electrodes | Products [Internet]. Blackrock Neurotech. [cited 2025 Mar 5]. Available from: https://blackrockneurotech.com/products/utah-array/

39. Marr D. MED Probe for Basic / Plex System [Internet]. med64.com. [cited 2025 Mar 5]. Available from: https://www.med64.com/products/med-probe-mea/med-probe-basic-plex/

40. High-Density Microelectrode Array (HD-MEA) | 3Brain [Internet]. [cited 2025 Mar 5]. Available from: https://www.3brain.com/

41. Single-well HD-MEA Platform | BioCAM DupleX | 3Brain [Internet]. [cited 2025 Mar 5]. Available from: https://www.3brain.com/products/single-well/biocam-duplex

42. Neuropixels NEW [Internet]. [cited 2025 Mar 5]. Home | Neuropixels. Available from: https://www.neuropixels.org

43. CerePort Plug, Standalone, Adaptors & Accessories | Products [Internet]. Blackrock Neurotech. [cited 2025 Mar 6]. Available from: https://blackrockneurotech.com/products/cereport-plug-standalone/

44. Flesher SN, Downey JE, Weiss JM, Hughes CL, Herrera AJ, Tyler-Kabara EC, et al. A brain-computer interface that evokes tactile sensations improves robotic arm control. Science. 2021 May 21;372[6544]:831–6.

45. Hochberg LR, Serruya MD, Friehs GM, Mukand JA, Saleh M, Caplan AH, et al. Neuronal ensemble control of prosthetic devices by a human with tetraplegia. Nature. 2006 Jul;442[7099]:164–71.

46. Davis TS, Wark H a. C, Hutchinson DT, Warren DJ, O'Neill K, Scheinblum T, et al. Restoring motor control and sensory feedback in people with upper extremity amputations using arrays of 96 microelectrodes implanted in the median and ulnar nerves. J Neural Eng. 2016 Jun;13[3]:036001.

47. Wilson GH, Stavisky SD, Willett FR, Avansino DT, Kelemen JN, Hochberg LR, et al. Decoding spoken English from intracortical electrode arrays in dorsal precentral gyrus. J Neural Eng. 2020 Nov 25;17[6]:066007.

48. Willett FR, Avansino DT, Hochberg LR, Henderson JM, Shenoy KV. High-performance brain-to-text communication via handwriting. Nature. 2021 May;593[7858]:249–54.

49. Hughes CL, Flesher SN, Weiss JM, Downey JE, Boninger M, Collinger JL, et al. Neural stimulation and recording performance in human sensorimotor cortex over 1500 days. J Neural Eng. 2021 Aug 13;18[4].

50. Magnusson Fredlund J. Literature Study on the Technical Development of Invasive Recording Brain Computer Interfaces. Proceedings of Clinical Innovations [Internet]. 2024 [cited 2025 Mar 14]; Available from: http://lup.lub.lu.se/student-papers/record/9158403

51. Du ZJ, Kolarcik CL, Kozai TDY, Luebben SD, Sapp SA, Zheng XS, et al. Ultrasoft microwire neural electrodes improve chronic tissue integration. Acta Biomaterialia. 2017 Apr 15;53:46–58.

52. Weltman A, Yoo J, Meng E. Flexible, Penetrating Brain Probes Enabled by Advances in Polymer Microfabrication. Micromachines. 2016 Oct;7[10]:180.

53. Yamashita K, Sawahata H, Yamagiwa S, Numano R, Koida K, Kawano T. Floating 5-μm-Diameter Needle for Low Invasive Chronic Recording. In: 2019 20th International Conference on Solid-State Sensors, Actuators and Microsystems & Eurosensors XXXIII (TRANSDUCERS & EUROSENSORS XXXIII) [Internet]. 2019 [cited 2025 Mar 6]. p. 302–5. Available from: https://ieeexplore.ieee.org/abstract/document/8808218

54. Mestais CS, Charvet G, Sauter-Starace F, Foerster M, Ratel D, Benabid AL. WIMAGINE: wireless 64-channel ECoG recording implant for long term clinical applications. IEEE Trans Neural Syst Rehabil Eng. 2015 Jan;23[1]:10–21.

55. Musk E. An Integrated Brain-Machine Interface Platform With Thousands of Channels. J Med Internet Res. 2019 Oct 31;21[10]:e16194.

56. Hanson TL, Diaz-Botia CA, Kharazia V, Maharbiz MM, Sabes PN. The “sewing machine” for minimally invasive neural recording [Internet]. bioRxiv; 2019 [cited 2025 Mar 6]. p. 578542. Available from: https://www.biorxiv.org/content/10.1101/578542v1

57. Shadmani A, Viswam V, Chen Y, Bounik R, Dragas J, Radivojevic M, et al. Stimulation and Artifact-suppression Techniques for in-vitro High-density Microelectrode Array Systems. IEEE Trans Biomed Eng. 2019 Sep;66[9]:2481–90.

58. Ross, Computer Networking a Top to Down Approach (GE) [Internet]. [cited 2024 Aug 7]. Available from: https://www.pearson.com/content/one-dot-com/one-dot-com/se/en/Nordics-Higher-Education/subject-catalogue/computer-science/ross-computer-networking-a-top-to-down-approach-ge.html

59. Peterson, L. L., & Davie, B. S. (2011). Computer Networks: A Systems Approach. Morgan Kaufmann. - Google Search [Internet]. [cited 2024 Aug 7]. Available from: https://www.google.com/search?q=Peterson%2C+L.+L.%2C+%26+Davie%2C+B.+S.+(2011).+Computer+Networks%3A+A+Systems+Approach.+Morgan+Kaufmann.&rlz=1C1ONGR_enUS1109US1109&sourceid=chrome&ie=UTF-8

60. Merrill DR, Bikson M, Jefferys JGR. Electrical stimulation of excitable tissue: design of efficacious and safe protocols. J Neurosci Methods. 2005 Feb 15;141[2]:171–98.

61. Rattay F. The basic mechanism for the electrical stimulation of the nervous system. Neuroscience. 1999 Mar;89[2]:335–46.

62. Thorpe S, Fize D, Marlot C. Speed of processing in the human visual system. Nature. 1996 Jun;381[6582]:520–2.

63. Lamme VA, Roelfsema PR. The distinct modes of vision offered by feedforward and recurrent processing. Trends Neurosci. 2000 Nov;23[11]:571–9.

64. Desmurget M, Grafton S. Forward modeling allows feedback control for fast reaching movements. Trends Cogn Sci. 2000 Nov 1;4[11]:423–31.

65. Blumenfeld Z, Brontë-Stewart H. High Frequency Deep Brain Stimulation and Neural Rhythms in Parkinson's Disease. Neuropsychol Rev. 2015 Dec 1;25[4]:384–97.

66. Beurrier C, Bioulac B, Audin J, Hammond C. High-Frequency Stimulation Produces a Transient Blockade of Voltage-Gated Currents in Subthalamic Neurons. Journal of Neurophysiology. 2001 Apr;85[4]:1351–6.

67. Reger BD, Fleming KM, Sanguineti V, Alford S, Mussa-Ivaldi FA. Connecting Brains to Robots: An Artificial Body for Studying the Computational Properties of Neural Tissues. Artificial Life. 2000 Oct 1;6[4]:307–24.

68. Andersen J, Revah O, Miura Y, Thom N, Amin ND, Kelley KW, et al. Generation of Functional Human 3D Cortico-Motor Assembloids. Cell. 2020 Dec 23;183[7]:1913-1929.e26.